

Accepted Manuscript

Design, synthesis, and biological activities of 1-aryl-(3-(2-styryl)phenyl)prop-2-en-1-ones

Soon Young Shin, Junho Lee, Jihyun Park, Youngshim Lee, Seunghyun Ahn, Ji Hye Lee, Dongsoo Koh, Young Han Lee, Yoongho Lim

PII: S0045-2068(18)30884-8
DOI: <https://doi.org/10.1016/j.bioorg.2018.11.005>
Reference: YBIOO 2613

To appear in: *Bioorganic Chemistry*

Received Date: 16 August 2018
Revised Date: 12 September 2018
Accepted Date: 5 November 2018

Please cite this article as: S. Young Shin, J. Lee, J. Park, Y. Lee, S. Ahn, J. Hye Lee, D. Koh, Y. Han Lee, Y. Lim, Design, synthesis, and biological activities of 1-aryl-(3-(2-styryl)phenyl)prop-2-en-1-ones, *Bioorganic Chemistry* (2018), doi: <https://doi.org/10.1016/j.bioorg.2018.11.005>

This is a PDF file of an unedited manuscript that has been accepted for publication. As a service to our customers we are providing this early version of the manuscript. The manuscript will undergo copyediting, typesetting, and review of the resulting proof before it is published in its final form. Please note that during the production process errors may be discovered which could affect the content, and all legal disclaimers that apply to the journal pertain.



Design, synthesis, and biological activities of 1-aryl-(3-(2-styryl)phenyl)prop-2-en-1-ones

Soon Young Shin^a, Junho Lee^b, Jihyun Park^b, Youngshim Lee^b, Seunghyun Ahn^b, Ji Hye Lee^c,
Dongsoo Koh^c, Young Han Lee^{a,*}, Yoongho Lim^{b,*}

^a*Department of Biological Sciences, Konkuk University, Seoul 05029, Korea*

^b*Division of Bioscience and Biotechnology, BBRC, Konkuk University, Seoul 05029, Korea*

^c*Department of Applied Chemistry, Dongduk Women's University, Seoul 02748, Korea*

***Corresponding authors:**

Prof. Yoongho Lim; Division of Bioscience and Biotechnology, Konkuk University

Hwayang-Dong 1, Kwangjin-Ku, Seoul, Korea 05029

Tel.: 82-2-450-3760; Fax : 82-2-3437-6106; Email: yoongho@konkuk.ac.kr

Prof. Young Han Lee; Department of Biological Sciences, Konkuk University,

Tel.: 82-2-2049-6115; Email: yhlee58@konkuk.ac.kr

Abbreviations: CoMFA, comparative molecular field analysis; CoMSIA, comparative molecular similarity index analysis; GI₅₀, half-maximal cell growth inhibitory concentration; SPP, 1-aryl-(3-(2-styryl)phenyl)prop-2-en-1-one; COSY, correlated spectroscopy; HMBC, heteronuclear multiple bonded connectivities; NOESY, nuclear Overhauser enhanced spectroscopy

Abstract

A moderate elevation in reactive oxygen species (ROS) levels can generally be controlled in normal cells, but may lead to death of cancer cells as the ROS level in cancer cells is already elevated. Therefore, a ROS-generating compound can act as a selective chemotherapeutic agent for cancer cells that does not affect normal cells. In our previous study, a compound containing a Michael acceptor was selectively cytotoxic to cancer cells without affecting normal cells; therefore, we designed and synthesized 26 compounds containing a Michael acceptor. Their cytotoxicities against HCT116 human colon cancer cell lines were measured by using a clonogenic long-term survival assay. To derive the structural conditions required to obtain stronger cytotoxicity against cancer cells, the relationships between the half-maximal cell growth inhibitory concentration values of the synthesized compounds and their physicochemical properties were evaluated by Comparative Molecular Field Analysis and Comparative Molecular Similarity Indices Analysis. It was confirmed that the compound with the best half-maximal cell growth inhibitory concentration triggered apoptosis through ROS generation, which then led to stimulation of the caspase pathway.

key words: 1-aryl-(3-(2-styryl)phenyl)prop-2-en-1-one; CoMFA; CoMSIA; ROS generation; poly(ADP-ribose) polymerase; apoptosis

1. Introduction

There are more than 100,000 publications containing “reactive oxygen species” (ROS) as a key word [1]. Triplet molecular oxygen in the ground state contains two valence electrons with parallel spins; conversion to ROS may occur by energy transfer or electron transfer reactions with organic molecules [2]. Molecular oxygen can be reduced to superoxide; dismutation of superoxide can produce hydrogen peroxide, which can then be reduced to hydroxyl radical. Superoxide, hydrogen peroxide, and hydroxyl radical are types of ROS. Triplet molecular oxygen may be converted to singlet oxygen by radiation, which is also a ROS [3]. ROS can be produced via radiolytic processes in exogenous conditions and via the defense mechanisms of cells and tissues in endogenous conditions [4]. The roles of ROS are known to be related to the defense system against microbial invasion; in addition, ROS are related to cell signal transduction and the cell cycle, including apoptosis, gene expression, and cell signaling cascades [5]. Although the moderate production of ROS can elevate cell proliferation and differentiation, excessive production can cause oxidative damage to biomolecules [6,7]. Consequently, the homeostasis of ROS is crucial for normal cell growth and survival [8]. To prevent cellular damage in normal conditions, the level of ROS is controlled; however, the level in cancer cells is higher than in normal cells [9]. This phenomenon induces cell death in cancer cells. Although a moderate elevation of ROS level can be controlled in normal cells, it may exceed the antioxidative ability of cancer cells, which results in the cancer cell death [9]. Therefore, ROS-generating compounds can act as selective chemotherapeutic agents against cancer cells that do

not affect normal cells [10]. Three such compounds, 2-(*p*-tolyl)-4*H*-benzo[*h*]chromen-4-one, 2-allyl-1-((3,4-dimethoxyphenethyl)amino)-3-methylbenzo[4,5]imidazo[1,2-*a*]pyridine-4-carbonitrile, and 3-(1-acetyl-5-(furan-2-yl)-4,5-dihydro-1*H*-pyrazol-3-yl)-6-chloro-4-phenylquinolin-2(1*H*)-one, have been reported as ROS enhancers [11]. Piperlongumine is known to be selectively toxic to cancer cells [12]. Based on the study of its analogs, it was suggested that the Michael acceptor moiety was important for ROS generation [13]. A Michael acceptor including α,β -unsaturated carbonyl group forms a covalent bond with glutathione (GSH) by a Michael addition. For GSH to quench ROS, it should be remained as a reduced form [14]. However, S-alkylation of GSH by a Michael addition with a Michael acceptor leads to loss of the possibility which GSH can be converted to its oxidized form [15]. This phenomenon prevents the elimination of ROS, which causes accumulation of ROS. In the authors' previous study, one compound, (*E*)-3-(3,5-dimethoxyphenyl)-1-(2-methoxyphenyl)prop-2-en-1-one, containing a Michael acceptor (Figure 1A) showed selective toxicity to cancer cells without affecting normal cells [16]. Therefore, we designed and synthesized 26 compounds containing Michael acceptors to find compounds able to generate ROS (Figure 1B). The design of the current compounds was based on the combination of chalcone (Figure 1C) and resveratrol (Figure 1D). Chalcone and resveratrol are secondary metabolites of plants. It has been reported that chalcone and resveratrol derivatives exert anticancer activities in *in vitro* and *in vivo* experiments [16-21]. Their structures were identified by using NMR spectroscopy and high-resolution mass spectrometry (HR/MS). It has been previously explained why ROS-generating compounds should be studied for the possible discovery of a chemotherapeutic agent. Therefore, the cytotoxicities of the designed compounds against HCT116 human colon cancer cell lines were measured by using a clonogenic

long-term survival assay [22]. The half-maximal cell growth inhibitory concentration (GI_{50}) was determined. The compound showing the best GI_{50} value, (*E*)-3-(2-((*E*)-4-methoxystyryl)-4,6-dimethoxyphenyl)-1-(pyridin-2-yl)prop-2-en-1-one, was subjected to further study to determine whether it stimulated ROS production, which was measured by using 2',7'-dichlorofluorescein diacetate dye. Further biological activities of the title compound were evaluated for the induction of apoptosis using annexin V staining. The aims of this study were to find compounds stimulating ROS generation and to determine the structural conditions that result in stronger cytotoxicity against cancer cells, as determined from quantitative structure-activity relationship (QSAR) calculations.

2. Materials and Methods

2.1. Preparation of 1-aryl-(3-(2-styryl)phenyl)prop-2-en-1-ones

We designed 26 derivatives of 1-aryl-(3-(2-styryl)phenyl)prop-2-en-1-one (named as SPP), as listed in Table 1. Their synthetic procedures are summarized in Scheme 1. In brief, 2 mL $POCl_3$ was added dropwise to a solution of *trans*-trimethoxystilbene **I** (2.7 g, 10 mmol) in 20 mL DMF in an ice-water bath and stirred overnight at room temperature. The resulting reaction mixture was poured into 400 mL ice-water and stirred for 1–2 h to yield a precipitate. The resulting solid was filtered, washed with water, and air-dried. For purification, recrystallization from hot methanol was performed to produce aldehyde compound **II** (yield: 30 %) and methyl aldehyde compound **III** (yield: 15 %) respectively. The aldehyde **II** or **III** was treated with methyl

aromatic ketone **IV** (1.2–1.5 eq.) in ethanol. An excess of 50% KOH solution was added to the reaction mixture and stirred at overnight at room temperature overnight. Precipitation was obtained by the addition of 3 N HCl until the pH reached 3–4. The resulting solids were filtered and washed with ethanol to yield the corresponding chalcone compounds 1–19 or 20–26, which were purified by recrystallization. The synthesis of derivative **13** was performed as follows: Compound **II** (284 mg, 0.95 mmol) and 2-acetylpyridine (180 mg, 1.48 mmol) were dissolved in 20 mL ethanol. To this reaction mixture, 2 mL aqueous (aq.) KOH (50 w/v %) was added and stirred at room temperature for 13 h. After completion of the reaction, the reaction mixture was acidified with 3 N HCl (pH = 3–4) to cause precipitation. The resulting solid was filtered and washed with ethanol. Color: lemon; m.p.: 157–158 °C; yield: 80%. Similarly, the synthesis of derivative **20** was performed as follows: Compound **III** (304 mg, 0.96 mmol) and 2-methoxyacetophenone (192 mg, 1.26 mmol) were dissolved in 20 mL ethanol. To the reaction mixture, 2 mL aq. KOH (50 w/v %) was added and stirred at room temperature for 28 h. After completion, the reaction mixture was acidified by the addition of 3 N HCl (pH = 3–4) to yield precipitation. The resulting solid was filtered and washed with ethanol. Recrystallization from hot methanol was performed, yielding analytically pure compound **20**. Color: yellow; m.p.: 94–100 °C; yield: 82%.

Synthetic SPP derivatives were identified by using nuclear magnetic resonance (NMR) spectroscopy, performed on an Avance 400 spectrometer system (9.4 T; Bruker, Karlsruhe, Germany) at 25 °C. The experimental methods followed a previous report [23]. To confirm the structural determination obtained from NMR spectroscopy, high-resolution mass spectrometry (HR/MS) was performed by using an ultraperformance liquid chromatography (UPLC)-hybrid

quadrupole time-of-flight mass spectrometer with a Waters Acquity UPLC system (Waters Corp., Milford, MA); assistance was provided by Prof. Choong Hwan Lee at Konkuk University, Korea [24]. All HR/MS data were collected in $[M+H]^+$ mode. The spectroscopic data of the 26 SPP derivatives synthesized for these studies are presented below.

(E)-3-(2-((E)-4-Methoxystyryl)-4,6-dimethoxyphenyl)-1-(2-methoxyphenyl)prop-2-en-1-one

(1)

Color: orange; m.p. 104–106 °C; yield 28%; ^1H NMR δ (in DMSO- d_6) 3.64(s, 3H), 3.80(s, 3H), 3.83(s, 3H), 3.84(s, 3H), 6.38(d, $J= 2.3$ Hz, 1H), 6.69(d, $J= 2.3$ Hz, 1H), 6.86(d, $J= 8.8$ Hz, 1H), 6.88(d, $J= 8.8$ Hz, 1H), 6.89(d, $J= 16.0$ Hz, 1H), 6.98(ddd, $J= 0.8, 7.4, 7.6$ Hz, 1H), 7.24(d, $J= 16.0$ Hz, 1H), 7.38(d, $J= 8.8$ Hz, 1H), 7.38(d, $J= 16.0$ Hz, 1H), 7.38(ddd, $J= 1.7, 7.4, 8.8$ Hz, 1H), 7.61 (dd, $J= 1.7, 7.6$ Hz, 1H), and 7.99(d, $J= 16.0$ Hz, 1H); ^{13}C NMR δ (in DMSO- d_6) 55.4, 55.5, 55.7, 97.6, 103.5, 111.6, 114.2, 116.1, 120.6, 125.5, 128.1, 129.7, 130.0, 130.2, 130.3, 131.4, 132.4, 138.3, 141.4, 158.0, 159.6, 160.8, 161.6, and 194.0; HR/MS calcd. for $\text{C}_{27}\text{H}_{26}\text{O}_5$ $(M+H)^+$ 431.1858, found 431.1865.

(E)-3-(2-((E)-4-Methoxystyryl)-4,6-dimethoxyphenyl)-1-(3-methoxyphenyl)prop-2-en-1-one

(2)

Color: yellow; m.p. 66–70 °C; yield 90%; ^1H NMR δ (in DMSO- d_6) 3.75(s, 3H), 3.78(s, 3H), 3.87(s, 3H), 3.91(s, 3H), 6.60(d, $J= 2.1$ Hz, 1H), 6.81(d, $J= 2.0$ Hz, 1H), 6.95(d, $J= 8.7$ Hz, 1H), 7.07(d, $J= 16.1$ Hz, 1H), 7.18(dd, $J= 2.6, 8.0$ Hz, 1H), 7.32(dd, $J= 7.7, 8.0$ Hz, 1H), 7.34(dd, $J= 1.6, 2.6$ Hz, 1H), 7.39(d, $J= 16.1$ Hz, 1H), 7.44(dd, $J= 1.6, 7.7$ Hz, 1H), 7.55(d, $J= 8.7$ Hz, 1H),

7.70(d, $J= 15.7$ Hz, 1H), and 8.02(d, $J= 15.7$ Hz, 1H); ^{13}C NMR δ (in DMSO- d_6) 55.2, 55.6, 55.8, 56.0, 97.8, 104.3, 112.5, 114.6, 118.9, 120.5, 122.3, 124.7, 128.1, 129.5, 130.0, 130.9, 132.0, 138.2, 139.6, 141.5, 159.4, 159.5, 160.8, 161.7, and 189.6; HR/MS calcd. for $\text{C}_{27}\text{H}_{26}\text{O}_5$ ($\text{M}+\text{H}$) $^+$ 431.1858, found 431.1887 [25].

(E)-3-(2-((E)-4-Methoxystyryl)-4,6-dimethoxyphenyl)-1-(4-methoxyphenyl)prop-2-en-1-one
(3)

Color: pale yellow; m.p. 118–124 °C; yield 92%; ^1H NMR δ (in DMSO- d_6) 3.77(s, 3H), 3.82(s, 3H), 3.87(s, 3H), 3.90(s, 3H), 6.59(d, $J= 2.1$ Hz, 1H), 6.80(d, $J= 2.1$ Hz, 1H), 6.95(d, $J= 8.6$ Hz, 1H), 6.99(d, $J= 8.8$ Hz, 1H), 7.06(d, $J= 16.5$ Hz, 1H), 7.34(d, $J= 16.5$ Hz, 1H), 7.54(d, $J= 8.6$ Hz, 1H), 7.56(d, $J= 15.8$ Hz, 1H), 7.93(d, $J= 8.8$ Hz, 1H), and 7.98(d, $J= 15.8$ Hz, 1H); ^{13}C NMR δ (in DMSO- d_6) 55.2, 55.5, 55.9, 97.8, 104.1, 114.0, 114.3, 114.8, 124.1, 124.8, 129.5, 130.4, 130.9, 131.0, 131.8, 137.2, 141.2, 159.3, 160.6, 161.5, 162.9, and 187.9; HR/MS calcd. for $\text{C}_{27}\text{H}_{26}\text{O}_5$ ($\text{M}+\text{H}$) $^+$ 431.1858, found 431.1867. [25]

(E)-3-(2-((E)-4-Methoxystyryl)-4,6-dimethoxyphenyl)-1-(2-hydroxy-5-methoxyphenyl)prop-2-en-1-one
(4)

Color: red orange; m.p. 138–144 °C; yield 25%; ^1H NMR δ (in DMSO- d_6) 3.66(s, 3H), 3.87(s, 3H), 3.99(s, 3H), 4.04(s, 3H), 6.71(d, $J= 1.5$ Hz, 1H), 6.93(d, $J= 1.5$ Hz, 1H), 6.99(d, $J= 8.3$ Hz, 1H), 7.02(d, $J= 8.5$ Hz, 1H), 7.19(d, $J= 16.1$ Hz, 1H), 7.21(dd, $J= 2.9, 8.3$ Hz, 1H), 7.37(d, $J= 2.9$ Hz, 1H), 7.52(d, $J= 16.1$ Hz, 1H), 7.67(d, $J= 8.5$ Hz, 1H), 7.82(d, $J= 15.5$ Hz, 1H), and 8.34(d, $J= 15.5$ Hz, 1H); ^{13}C NMR δ (in DMSO- d_6) 55.3, 55.4, 55.6, 56.0, 97.8, 104.9, 112.1,

114.5, 115.1, 119.2, 120.6, 123.0, 124.4, 125.2, 128.5, 130.1, 132.7, 139.5, 142.6, 152.2, 157.3, 160.1, 161.7, 162.9, and 194.0; HR/MS calcd. for $C_{27}H_{26}O_6$ (M+H)⁺ 447.1808, found 447.1770.

(E)-3-(2-((E)-4-Methoxystyryl)-4,6-dimethoxyphenyl)-1-(2-hydroxy-4-methoxyphenyl)prop-2-en-1-one (5)

Color: brown; m.p. 148–152 °C; yield 30%; ¹H NMR δ (in DMSO-d₆) 3.78(s, 3H), 3.81(s, 3H), 3.88(s, 3H), 3.93(s, 3H), 6.43(dd, *J* = 9.1, 2.5 Hz, 1H), 6.49(d, *J* = 2.5 Hz, 1H), 6.60(d, *J* = 2.3 Hz, 1H), 6.81(d, *J* = 2.3 Hz, 1H), 6.96(d, *J* = 8.7 Hz, 1H), 7.07(d, *J* = 16.0 Hz, 1H), 7.37(d, *J* = 16.0 Hz, 1H), 7.56(d, *J* = 8.7 Hz, 1H), 7.69(d, *J* = 15.4 Hz, 1H), 7.80(d, *J* = 9.1 Hz, 1H), and 8.10(d, *J* = 15.4 Hz, 1H); ¹³C NMR δ (in DMSO-d₆) 55.2, 55.6, 55.7, 56.0, 97.8, 101.0, 104.3, 107.4, 114.0, 114.3, 114.5, 122.5, 124.5, 128.2, 129.5, 131.6, 132.3, 137.9, 141.8, 159.4, 161.0, 161.9, 165.6, 165.7, and 191.9; HR/MS calcd. for $C_{27}H_{26}O_6$ (M+H)⁺ 447.1808, found 447.1801.

(E)-3-(2-((E)-4-Methoxystyryl)-4,6-dimethoxyphenyl)-1-(2-hydroxyphenyl)prop-2-en-1-one (6)

Color: yellow; m.p. 136–140 °C; yield 48%; ¹H NMR δ (in DMSO-d₆) 3.78(s, 3H), 3.89(s, 3H), 3.94(s, 3H), 6.62(d, *J* = 2.2 Hz, 1H), 6.83(d, *J* = 2.2 Hz, 1H), 6.90(dd, *J* = 7.2, 8.0 Hz, 1H), 6.96(d, *J* = 8.7 Hz, 1H), 6.98(d, *J* = 8.8 Hz, 1H), 7.08(d, *J* = 16.1 Hz, 1H), 7.38(d, *J* = 16.1 Hz, 1H), 7.52(ddd, *J* = 1.2, 7.2, 8.8 Hz, 1H), 7.56(d, *J* = 8.7 Hz, 1H), 7.73(d, *J* = 15.5 Hz, 1H), 7.84(dd, *J* = 1.2, 8.0 Hz, 1H), and 8.12(d, *J* = 15.5 Hz, 1H); ¹³C NMR δ (in DMSO-d₆) 55.2, 55.6, 56.1, 97.8, 104.3, 114.3, 114.4, 117.8, 119.2, 121.1, 123.0, 124.4, 128.2, 129.4, 129.9, 132.4, 135.9, 138.8, 142.0, 159.4, 161.1, 161.6, 162.1, and 193.9; HR/MS calcd. for $C_{26}H_{24}O_5$ (M+H)⁺ 417.1702, found 417.1692.

(E)-3-(2-((E)-4-Methoxystyryl)-4,6-dimethoxyphenyl)-1-(4-hydroxyphenyl)prop-2-en-1-one (7)

Color: orange; m.p. 162–166 °C; yield 26%; ¹H NMR δ (in DMSO-d₆) 3.77(s, 3H), 3.86(s, 3H), 3.90(s, 3H), 6.58(d, *J*= 1.7 Hz, 1H), 6.79(d, *J*= 1.7 Hz, 1H), 6.83(d, *J*= 8.5 Hz, 1H), 6.95(d, *J*= 8.4 Hz, 1H), 7.05(d, *J*= 16.1 Hz, 1H), 7.33(d, *J*= 16.1 Hz, 1H), 7.53(d, *J*= 15.6 Hz, 1H), 7.54(d, *J*= 8.4 Hz, 1H), 7.85(d, *J*= 8.5 Hz, 1H), 7.95(d, *J*= 15.6 Hz, 1H), and 10.39(s, 1H); ¹³C NMR δ (in DMSO-d₆) 55.3, 55.5, 56.0, 97.8, 104.1, 114.3, 115.0, 115.5, 124.3, 125.0, 128.1, 129.6, 130.8, 131.8, 137.4, 141.2, 159.4, 160.6, 161.5, 162.0, and 187.8; HR/MS calcd. for C₂₆H₂₄O₅ (M+H)⁺ 417.1702, found 417.1672 [26].

(E)-3-(2-((E)-4-Methoxystyryl)-4,6-dimethoxyphenyl)-1-(2-hydroxy-5-nitrophenyl)prop-2-en-1-one (8)

Color: orange; m.p. 168–172 °C; yield 48%; ¹H NMR δ (in DMSO-d₆) 3.85(s, 3H), 3.93(s, 3H), 4.00(s, 3H), 6.47(d, *J*= 1.6 Hz, 1H), 6.74(d, *J*= 1.6 Hz, 1H), 6.92(d, *J*= 8.5 Hz, 1H), 6.95(d, *J*= 16.0 Hz, 1H), 7.08(d, *J*= 9.2 Hz, 1H), 7.35(d, *J*= 16.0 Hz, 1H), 7.50(d, *J*= 8.5 Hz, 1H), 7.89(d, *J*= 15.2 Hz, 1H), 8.31(dd, *J*= 2.4, 9.2 Hz, 1H), 8.39(d, *J*= 15.2 Hz, 1H), and 8.80(d, *J*= 2.4 Hz, 1H); ¹³C NMR δ (in DMSO-d₆) 55.5, 55.7, 56.1, 97.9, 104.6, 114.3, 114.5, 115.1, 119.5, 120.5, 124.6, 126.3, 128.3, 129.7, 130.5, 133.5, 139.6, 141.9, 143.8, 160.1, 162.0, 163.0, 168.6, and 193.8; HR/MS calcd. for C₂₆H₂₃NO₇ (M+H)⁺ 462.1553, found 462.1559.

(E)-3-(2-((E)-4-ethoxystyryl)-4,6-dimethoxyphenyl)-1-(5-bromo-2-hydroxyphenyl)prop-2-en-1-one (9)

Color: orange; m.p. 156–160 °C; yield 27%; ^1H NMR δ (in DMSO- d_6) 3.86(s, 3H), 3.99(s, 3H), 4.04(s, 3H), 6.70(d, J = 2.2 Hz, 1H), 6.95(d, J = 2.2 Hz, 1H), 7.02(d, J = 8.7 Hz, 1H), 7.04(d, J = 8.7 Hz, 1H), 7.19(d, J = 16.3 Hz, 1H), 7.54(d, J = 16.3 Hz, 1H), 7.67(d, J = 8.7 Hz, 1H), 7.70(dd, J = 2.3, 8.7 Hz, 1H), 7.81(d, J = 15.5 Hz, 1H), 8.05(d, J = 2.3 Hz, 1H), 8.31(d, J = 15.5 Hz, 1H), and 11.97(s, 1H); ^{13}C NMR δ (in DMSO- d_6) 55.4, 55.8, 56.3, 98.1, 105.0, 110.5, 114.8, 115.3, 120.8, 123.5, 123.6, 125.1, 128.7, 130.3, 132.5, 133.1, 138.5, 140.2, 143.0, 160.3, 161.8, 162.0, 163.2, and 193.5; HR/MS calcd. for $\text{C}_{26}\text{H}_{23}\text{BrO}_5$ ($\text{M}+\text{H}$) $^+$ 495.0807, found 495.0826.

(E)-3-(2-((E)-4-Methoxystyryl)-4,6-dimethoxyphenyl)-1-(4-fluoro-2-hydroxyphenyl)prop-2-en-1-one (10)

Color: orange; m.p. 195–200 °C; yield 89%; ^1H NMR δ (in DMSO- d_6) 3.75(s, 3H), 3.85(s, 3H), 3.86(s, 3H), 6.28(dd, J = 2.5, 8.5 Hz, 1H), 6.44(dd, J = 2.5, 12.4 Hz, 1H), 6.56(d, J = 2.3 Hz, 1H), 6.82(d, J = 2.3 Hz, 1H), 6.92(d, J = 8.8 Hz, 1H), 7.07(d, J = 16.1 Hz, 1H), 7.38(d, J = 16.1 Hz, 1H), 7.54(d, J = 8.8 Hz, 1H), 7.69(dd, J = 8.0, 8.8 Hz, 1H), 7.87(d, J = 15.8 Hz, 1H), and 7.92(d, J = 15.8 Hz, 1H); ^{13}C NMR δ (in DMSO- d_6) 55.1, 55.4, 55.8, 97.7, 104.8, 103.6, 105.5, 114.2, 115.7, 122.0, 124.6, 125.2, 128.2, 129.6, 131.6, 132.7, 137.1, 140.6, 159.2, 160.4, 161.1, 165.1, 169.3, and 191.0; HR/MS calcd. for $\text{C}_{26}\text{H}_{23}\text{FO}_5$ ($\text{M}+\text{H}$) $^+$ 435.1596, found 435.1577.

(E)-3-(2-((E)-4-Methoxystyryl)-4,6-dimethoxyphenyl)-1-(5-fluoro-2-hydroxyphenyl)prop-2-en-1-one (11)

Color: orange; m.p. 154–156 °C; yield 80%; ^1H NMR δ (in DMSO- d_6) 3.85(s, 3H), 3.98(s, 3H), 4.02(s, 3H), 6.68(d, J = 2.2 Hz, 1H), 6.93(d, J = 2.2 Hz, 1H), 7.00(d, J = 8.7 Hz, 1H), 7.06(dd, J =

4.6, 9.1 Hz, 1H), 7.18(d, $J= 16.1$ Hz, 1H), 7.40(ddd, $J= 3.2, 8.0, 9.1$ Hz, 1H), 7.53(d, $J= 16.1$ Hz, 1H), 7.66(d, $J= 8.7$ Hz, 1H), 7.71(dd, $J= 3.2, 9.2$ Hz, 1H), 7.86(d, $J= 15.5$ Hz, 1H), and 8.29(d, $J= 15.4$ Hz, 1H); ^{13}C NMR δ (in DMSO- d_6) 55.6, 56.0, 56.3, 98.7, 105.1, 114.8, 115.5, 115.7, 120.2, 122.3, 123.5, 123.7, 125.0, 128.8, 130.7, 133.2, 140.0, 143.5, 157.0, 160.0, 160.9, 162.7, 163.6, and 194.3; HR/MS calcd. for $\text{C}_{26}\text{H}_{23}\text{FO}_5$ ($\text{M}+\text{H}$) $^+$ 435.1232, found 435.1219.

(E)-3-(2-((E)-4-Methoxystyryl)-4,6-dimethoxyphenyl)-1-(5-chloro-2-hydroxyphenyl)prop-2-en-1-one (12)

Color: yellow; m.p. 156–160 °C; yield 76%; ^1H NMR δ (in DMSO- d_6) 3.84(s, 3H), 3.89(s, 3H), 3.93(s, 3H), 6.41(d, $J= 2.2$ Hz, 1H), 6.69(d, $J= 2.2$ Hz, 1H), 6.92(d, $J= 8.7$ Hz, 1H), 6.93(d, $J= 16.0$ Hz, 1H), 6.95(d, $J= 8.9$ Hz, 1H), 7.30(d, $J= 16.0$ Hz, 1H), 7.37(dd, $J= 2.5, 8.9$ Hz, 1H), 7.48(d, $J= 8.7$ Hz, 1H), 7.62(d, $J= 15.4$ Hz, 1H), 7.71(d, $J= 2.5$ Hz, 1H), 8.30(d, $J= 15.4$ Hz, 1H); ^{13}C NMR δ (in DMSO- d_6) 55.5, 55.6, 55.9, 97.7, 104.3, 114.5, 115.4, 120.1, 121.2, 121.7, 123.4, 125.1, 128.2, 128.9, 129.7, 132.6, 135.7, 140.5, 142.9, 159.9, 161.4, 162.1, 162.4, and 193.6; HR/MS calcd. for $\text{C}_{26}\text{H}_{23}\text{ClO}_5$ ($\text{M}+\text{H}$) $^+$ 451.1312, found 451.1246.

(E)-3-(2-((E)-4-Methoxystyryl)-4,6-dimethoxyphenyl)-1-(2-hydroxynaphthalen-1-yl)prop-2-en-1-one (13)

Color: red orange; m.p. 146–150 °C; yield 48%; ^1H NMR δ (in DMSO- d_6) 3.80(s, 3H), 3.84(s, 3H), 3.87(s, 3H), 6.57(d, $J= 2.2$ Hz, 1H), 6.79(d, $J= 2.2$ Hz, 1H), 6.85(d, $J= 16.1$ Hz, 1H), 6.91(d, $J= 8.7$ Hz, 1H), 6.96(d, $J= 16.1$ Hz, 1H), 7.10(d, $J= 16.1$ Hz, 1H), 7.14(d, $J= 8.7$ Hz, 1H), 7.25(d, $J= 8.9$ Hz, 1H), 7.35(ddd, $J= 1.4, 6.9, 8.2$ Hz, 1H), 7.44(ddd, $J= 1.4, 6.9, 8.2$ Hz, 1H), 7.58(d, $J=$

8.1 Hz, 1H), 7.61(d, $J= 16.1$ Hz, 1H), 7.90(d, $J= 8.2$ Hz, 1H), 7.90(d, $J= 8.9$ Hz, 1H), and 10.21(s, 1H); ^{13}C NMR δ (in DMSO- d_6) 55.2, 55.5, 55.9, 97.9, 103.6, 113.7, 114.2, 118.3, 120.2, 123.0, 123.1, 123.4, 127.1, 127.6, 127.9, 128.2, 129.1, 130.7, 130.8, 131.6, 132.0, 139.7, 140.8, 152.4, 159.3, 160.7, 161.8, and 197.7; HR/MS calcd. for $\text{C}_{30}\text{H}_{26}\text{O}_5$ ($\text{M}+\text{H}$) $^+$ 467.1858, found 467.1822.

(E)-3-(2-((E)-4-Methoxystyryl)-4,6-dimethoxyphenyl)-1-(thiophen-2-yl)prop-2-en-1-one (14)

Color: yellow; m.p. 140–144 °C; yield 71%; ^1H NMR δ (in DMSO- d_6) 3.78(s, 3H), 3.88(s, 3H), 3.93(s, 3H), 6.61(d, $J= 2.0$ Hz, 1H), 6.82(d, $J= 2.0$ Hz, 1H), 6.96(d, $J= 8.5$ Hz, 1H), 7.08(d, $J= 16.1$ Hz, 1H), 7.23(ddd, $J= 0.8, 3.8, 5.0$ Hz, 1H), 7.36(d, $J= 16.1$ Hz, 1H), 7.54(d, $J= 15.2$ Hz, 1H), 7.56(d, $J= 8.5$ Hz, 1H), 7.90(dd, $J= 0.8, 5.0$ Hz, 1H), 8.00(dd, $J= 0.8, 3.8$ Hz, 1H), and 8.01(d, $J= 15.2$ Hz, 1H); ^{13}C NMR δ (in DMSO- d_6) 55.2, 55.5, 56.0, 97.8, 104.2, 114.3, 114.4, 123.6, 124.4, 128.1, 128.9, 129.5, 132.2, 134.9, 137.2, 141.6, 145.6, 159.4, 160.8, 161.8, and 181.8; HR/MS calcd. for $\text{C}_{24}\text{H}_{22}\text{O}_4\text{S}$ ($\text{M}+\text{H}$) $^+$ 407.1283, found 407.1280.

(E)-3-(2-((E)-4-Methoxystyryl)-4,6-dimethoxyphenyl)-1-(thiophen-3-yl)prop-2-en-1-one (15)

Color: yellow; m.p. 122–125 °C; yield 83%; ^1H NMR δ (in DMSO- d_6) 3.83(s, 3H), 3.88(s, 3H), 3.89(s, 3H), 6.42(d, $J= 2.2$ Hz, 1H), 6.72(d, $J= 2.2$ Hz, 1H), 6.89(d, $J= 8.3$ Hz, 1H), 6.93(d, $J= 16.1$ Hz, 1H), 7.43(d, $J= 15.7$ Hz, 1H), 7.46(d, $J= 8.3$ Hz, 1H), 7.53(dd, $J= 0.9, 4.9$ Hz, 1H), 7.73(dd, $J= 2.6, 4.9$ Hz, 1H), 7.76(d, $J= 16.1$ Hz, 1H), 8.03(dd, $J= 0.9, 2.6$ Hz, 1H), and 8.18(d, $J= 15.7$ Hz, 1H); ^{13}C NMR δ (in DMSO- d_6) 55.5, 55.6, 55.8, 97.7, 103.8, 114.4, 116.1, 125.1,

126.0, 126.3, 127.6, 128.1, 128.5, 129.9, 131.7, 138.2, 141.8, 143.7, 159.8, 160.9, 161.7, and 184.7; HR/MS calcd. for C₂₄H₂₂O₄S (M+H)⁺ 407.1283, found 407.1281.

(E)-3-(2-((E)-4-Methoxystyryl)-4,6-dimethoxyphenyl)-1-(1H-pyrrol-2-yl)prop-2-en-1-one (16)

Color: yellow; m.p. 182–184 °C; yield 20%; ¹H NMR δ (in DMSO-d₆) 3.77(s, 3H), 3.87(s, 3H), 3.90(s, 3H), 6.19(dd, *J*= 2.1, 3.6 Hz, 1H), 6.59(d, *J*= 2.0 Hz, 1H), 6.81(d, *J*= 2.0 Hz, 1H), 6.90(m, 1H), 6.94(d, *J*= 8.7 Hz, 1H), 7.08(d, *J*= 16.1 Hz, 1H), 7.13(m, 1H), 7.33(d, *J*= 16.1 Hz, 1H), 7.35(d, *J*= 15.7 Hz, 1H), 7.54(d, *J*= 8.7 Hz, 1H), 7.93(d, *J*= 15.7 Hz, 1H), and 11.93(s, 1H); ¹³C NMR δ (in DMSO-d₆) 55.2, 55.5, 55.9, 97.8, 103.9, 110.0, 114.2, 115.0, 116.0, 124.9, 125.4, 126.0, 128.0, 129.5, 131.5, 133.1, 134.6, 140.6, 159.3, 160.3, 161.1, and 178.3; HR/MS calcd. for C₂₄H₂₃NO₄ (M+H)⁺ 390.1705, found 390.1738.

(E)-3-(2-((E)-4-Methoxystyryl)-4,6-dimethoxyphenyl)-1-(thiazol-2-yl)prop-2-en-1-one (17)

Color: yellow; m.p. 160–162 °C; yield 60%; ¹H NMR δ (in DMSO-d₆) 3.84(s, 3H), 3.90(s, 3H), 3.94(s, 3H), 6.44(d, *J*= 2.3 Hz, 1H), 6.74(d, *J*= 2.3 Hz, 1H), 6.91(d, *J*= 8.7 Hz, 1H), 6.96(d, *J*= 16.0 Hz, 1H), 7.42(d, *J*= 16.0 Hz, 1H), 7.52(d, *J*= 8.7 Hz, 1H), 7.64(d, *J*= 3.0 Hz, 1H), 8.00(d, *J*= 3.0 Hz, 1H), 8.00(d, *J*= 16.0 Hz, 1H), and 8.45(d, *J*= 16.0 Hz, 1H); ¹³C NMR δ (in DMSO-d₆) 55.5, 55.6, 55.9, 97.7, 103.9, 114.3, 115.9, 123.4, 125.2, 125.9, 128.4, 130.1, 132.4, 140.3, 142.8, 144.8, 159.8, 161.6, 162.3, 169.6, and 182.8; HR/MS calcd. for C₂₃H₂₁NO₄S (M+H)⁺ 408.1270, found 408.1283.

(E)-3-(2-((E)-4-Methoxystyryl)-4,6-dimethoxyphenyl)-1-(furan-2-yl)prop-2-en-1-one (18)

Color: yellow; m.p. 182–184 °C; yield 20%; ^1H NMR δ (in DMSO- d_6) 3.78(s, 3H), 3.88(s, 3H), 3.92(s, 3H), 6.60(d, J = 2.2 Hz, 1H), 6.73(dd, J = 1.5, 3.4 Hz, 1H), 6.82(d, J = 2.2 Hz, 1H), 6.96(d, J = 8.7 Hz, 1H), 7.07(d, J = 16.1 Hz, 1H), 7.35(d, J = 16.1 Hz, 1H), 7.42(dd, J = 0.9, 3.4 Hz, 1H), 7.45(d, J = 15.8 Hz, 1H), 7.55(d, J = 8.7 Hz, 1H), 7.99(dd, J = 0.9, 1.5 Hz, 1H), and 8.01(d, J = 15.8 Hz, 1H); ^{13}C NMR δ (in DMSO- d_6) 55.2, 55.5, 56.0, 97.8, 104.2, 112.8, 114.3, 114.4, 118.0, 123.5, 124.5, 128.1, 129.5, 132.2, 136.8, 141.6, 147.8, 155.3, 159.4, 160.8, 161.7, and 177.5; HR/MS calcd. for $\text{C}_{24}\text{H}_{22}\text{O}_5$ ($\text{M}+\text{H}$) $^+$ 391.1545, found 391.1548.

(E)-3-(2-((E)-4-Methoxystyryl)-4,6-dimethoxyphenyl)-1-(pyridin-2-yl)prop-2-en-1-one (19)

Color: yellow; m.p. 157–158 °C; yield 80%; ^1H NMR δ (in DMSO- d_6) 3.80(s, 3H), 3.86(s, 3H), 3.88(s, 3H), 6.40(d, J = 2.3 Hz, 1H), 6.71(d, J = 2.3 Hz, 1H), 6.87(d, J = 8.7 Hz, 1H), 6.94(d, J = 16.2 Hz, 1H), 7.39(ddd, J = 0.8, 4.8, 7.8 Hz, 1H), 7.42(d, J = 16.2 Hz, 1H), 7.52(d, J = 8.7 Hz, 1H), 7.80(ddd, J = 1.6, 7.8, 7.8 Hz, 1H), 8.14(dd, J = 0.8, 7.8 Hz, 1H), 8.22(d, J = 16.1 Hz, 1H), 8.32(d, J = 16.1 Hz, 1H), and 8.62(dd, J = 1.6, 4.8 Hz, 1H); ^{13}C NMR δ (in DMSO- d_6) 55.5, 55.6, 55.9, 97.6, 103.7, 114.2, 116.5, 122.9, 124.4, 125.9, 126.6, 128.4, 130.2, 131.7, 136.2, 138.9, 142.1, 149.0, 155.0, 159.7, 161.2, 161.8, and 190.5; HR/MS calcd. for $\text{C}_{25}\text{H}_{23}\text{NO}_4$ ($\text{M}+\text{H}$) $^+$ 402.1705, found 402.1667.

(E)-3-(2-((E)-4-Methoxystyryl)-4,6-dimethoxy-3-methylphenyl)-1-(2-methoxyphenyl)prop-2-en-1-one (20)

Color: pale yellow; m.p. 96–100 °C; yield 82%; ^1H NMR δ (in DMSO- d_6) 2.11(s, 3H), 3.67(s, 3H), 3.82(s, 3H), 3.86(s, 3H), 3.90(s, 3H), 6.34(d, J = 16.6 Hz, 1H), 6.41(s, 1H), 6.75(dd, J = 0.8,

7.9 Hz, 1H), 6.76(ddd, $J= 0.8, 7.6, 7.7$ Hz, 1H), 6.84(d, $J= 16.6$ Hz, 1H), 6.86(dd, $J= 1.8, 8.7$ Hz, 1H), 7.22(ddd, $J= 1.8, 7.6, 7.9$ Hz, 1H), 7.29(dd, $J= 1.8, 8.7$ Hz, 1H), 7.36(dd, $J= 1.8, 7.7$ Hz, 1H), 7.44(d, $J= 16.1$ Hz, 1H), and 7.78(d, $J= 16.1$ Hz, 1H); ^{13}C NMR δ (in DMSO- d_6) 12.7, 55.5, 55.6, 55.7, 93.8, 111.5, 114.1, 115.1, 117.5, 120.4, 124.4, 127.9, 129.2, 129.6, 129.8, 130.0, 131.5, 136.2, 142.2, 142.5, 157.4, 159.3, 159.6, 159.8, and 196.3; HR/MS calcd. for $\text{C}_{28}\text{H}_{28}\text{O}_5$ (M+H) $^+$ 445.2015, found 445.2058.

(E)-3-(2-((E)-4-Methoxystyryl)-4,6-dimethoxy-3-methylphenyl)-1-(3-methoxyphenyl)prop-2-en-1-one (21)

Color: yellow; m.p. 116–120 °C; yield 14%; ^1H NMR δ (in DMSO- d_6) 2.09(s, 3H), 3.75(s, 3H), 3.78(s, 3H), 3.91(s, 3H), 3.99(s, 3H), 6.41(d, $J= 16.6$ Hz, 1H), 6.70(s, 1H), 6.95(d, $J= 8.8$ Hz, 1H), 7.13(d, $J= 16.6$ Hz, 1H), 7.14(dd, $J= 2.6, 8.0$ Hz, 1H), 7.32(dd, $J= 7.7, 8.0$ Hz, 1H), 7.34(dd, $J= 1.6, 2.6$ Hz, 1H), 7.45(dd, $J= 1.6, 7.7$ Hz, 1H), 7.53(d, $J= 8.8$ Hz, 1H), 7.71(d, $J= 15.7$ Hz, 1H), and 8.00(d, $J= 15.7$ Hz, 1H); ^{13}C NMR δ (in DMSO- d_6) 12.5, 55.1, 55.2, 55.8, 55.9, 94.5, 112.3, 113.9, 114.2, 116.3, 118.5, 120.4, 122.3, 124.2, 127.8, 129.3, 129.8, 135.5, 139.8, 140.4, 141.9, 159.3, 159.4, 159.8, and 189.7; HR/MS calcd. for $\text{C}_{28}\text{H}_{28}\text{O}_5$ (M+H) $^+$ 445.2015, found 445.2017.

(E)-3-(2-((E)-4-Methoxystyryl)-4,6-dimethoxy-3-methylphenyl)-1-(4-methoxyphenyl)prop-2-en-1-one (22)

Color: yellow; m.p. 138–144 °C; yield 45%; ^1H NMR δ (in DMSO- d_6) 2.16(s, 3H), 3.79(s, 3H), 3.81(s, 3H), 3.88(s, 3H), 3.93(s, 3H), 6.44(s, 1H), 6.46(d, $J= 16.5$ Hz, 1H), 6.79(d, $J= 8.8$ Hz,

1H), 6.88(d, $J= 8.6$ Hz, 1H), 6.99(d, $J= 16.5$ Hz, 1H), 7.43(d, $J= 8.6$ Hz, 1H), 7.69(d, $J= 15.8$ Hz, 1H), 7.88(d, $J= 8.8$ Hz, 1H), and 8.08(d, $J= 15.8$ Hz, 1H); ^{13}C NMR δ (in DMSO- d_6) 12.8, 55.5, 55.7, 55.9, 93.9, 113.7, 114.3, 115.6, 117.6, 124.3, 124.9, 127.9, 130.1, 130.8, 131.9, 136.0, 140.4, 142.0, 159.1, 159.7, 159.8, 162.9, and 190.5; HR/MS calcd. for $\text{C}_{28}\text{H}_{28}\text{O}_5$ ($\text{M}+\text{H}$) $^+$ 445.2015, found 445.2028.

(E)-3-(2-((E)-4-Methoxystyryl)-4,6-dimethoxy-3-methylphenyl)-1-(2-hydroxy-5-methoxyphenyl) prop-2-en-1-one (23)

Color: orange brown; m.p. 182–186 °C; yield 80%; ^1H NMR δ (in DMSO- d_6) 2.20(s, 3H), 3.62(s, 3H), 3.84(s, 3H), 3.93(s, 3H), 3.98(s, 3H), 6.48(s, 1H), 6.50(d, $J= 16.5$ Hz, 1H), 6.92(d, $J= 9.0$ Hz, 1H), 6.92(ddd, $J= 2.4, 3.0, 8.8$ Hz, 1H), 7.05(d, $J= 16.5$ Hz, 1H), 7.07(dd, $J= 3.0, 9.0$ Hz, 1H), 7.24(d, $J= 3.0$ Hz, 1H), 7.48(ddd, $J= 2.4, 3.0, 8.8$ Hz, 1H), 7.84(d, $J= 15.5$ Hz, 1H), 8.30(d, $J= 15.5$ Hz, 1H), and 12.70(s, 1H); ^{13}C NMR δ (in DMSO- d_6) 12.8, 55.5, 55.8, 56.0, 93.8, 112.6, 114.4, 115.3, 118.0, 119.2, 120.2, 121.5, 123.6, 124.5, 128.1, 129.9, 136.4, 141.8, 142.4, 151.7, 158.0, 159.6, 159.9, 160.5, and 194.4; HR/MS calcd. for $\text{C}_{28}\text{H}_{28}\text{O}_6$ ($\text{M}+\text{H}$) $^+$ 461.1600, found 461.1611.

(E)-3-(2-((E)-4-Methoxystyryl)-4,6-dimethoxy-3-methylphenyl)-1-(3,4-dimethoxyphenyl)prop-2-en-1-one (24)

Color: yellow; m.p. 146–149 °C; yield 25%; ^1H NMR δ (in DMSO- d_6) 2.16(s, 3H), 3.80(s, 3H), 3.84(s, 3H), 3.88(s, 3H), 3.90(s, 3H), 3.93(s, 3H), 6.44(s, 1H), 6.46(d, $J= 16.5$ Hz, 1H), 6.68(d, $J= 8.3$ Hz, 1H), 6.87(dd, $J= 1.9, 8.7$ Hz, 1H), 6.99(d, $J= 16.5$ Hz, 1H), 7.42(dd, $J= 1.9, 8.7$ Hz,

1H), 7.49(dd, $J= 1.9, 8.3$ Hz, 1H), 7.51(d, $J= 1.9$ Hz, 1H), 7.70(d, $J= 15.8$ Hz, 1H), and 8.09(d, $J= 15.8$ Hz, 1H); ^{13}C NMR δ (in DMSO- d_6) 12.8, 55.5, 55.7, 55.9, 56.0, 56.1, 93.9, 110.0, 110.9, 114.3, 115.6, 117.6, 123.0, 124.0, 124.9, 127.9, 130.1, 132.1, 136.0, 140.3, 142.0, 149.1, 152.7, 159.1, 159.7, 159.8, and 190.2; HR/MS calcd. for $\text{C}_{29}\text{H}_{30}\text{O}_6$ (M+H) $^+$ 475.2121, found 475.2127.

(E)-3-(2-((E)-4-Methoxystyryl)-4,6-dimethoxy-3-methylphenyl)-1-(3-hydroxyphenyl)prop-2-en-1-one (25)

Color: yellow; m.p. 150–154 °C; yield 48%; ^1H NMR δ (in DMSO- d_6) 2.09(s, 3H), 3.78(s, 3H), 3.91(s, 3H), 3.99(s, 3H), 6.41(d, $J= 16.5$ Hz, 1H), 6.71(s, 1H), 6.95(d, $J= 8.8$ Hz, 1H), 6.97(d, $J= 8.1$ Hz, 1H), 7.14(d, $J= 16.5$ Hz, 1H), 7.22(dd, $J= 8.1, 8.1$ Hz, 1H), 7.28(s, 1H), 7.29(d, $J= 8.1$ Hz, 1H), 7.54(d, $J= 8.8$ Hz, 1H), 7.70(d, $J= 15.8$ Hz, 1H), 7.95(d, $J= 15.8$ Hz, 1H), and 9.85(s, 1H); ^{13}C NMR δ (in DMSO- d_6) 12.5, 55.3, 55.9, 56.0, 94.6, 113.9, 114.2, 114.3, 116.3, 118.9, 119.7, 122.4, 124.2, 127.9, 129.3, 129.8, 135.6, 139.8, 140.2, 142.0, 157.7, 159.3, 159.4, 159.7, and 190.0; HR/MS calcd. for $\text{C}_{27}\text{H}_{26}\text{O}_5$ (M+H) $^+$ 431.1858, found 431.1846.

(E)-3-(2-((E)-4-Methoxystyryl)-4,6-dimethoxy-3-methylphenyl)-1-(thiophen-2-yl)prop-2-en-1-one (26)

Color: yellow; m.p. 174–176 °C; yield 20%; ^1H NMR δ (in DMSO- d_6) 2.18(s, 3H), 3.87(s, 3H), 4.01(s, 3H), 4.11(s, 3H), 6.55(d, $J= 16.4$ Hz, 1H), 6.84(s, 1H), 7.02(d, $J= 8.6$ Hz, 1H), 7.23(dd, $J= 3.8, 4.9$ Hz, 1H), 7.26(d, $J= 16.4$ Hz, 1H), 7.64(d, $J= 8.6$ Hz, 1H), 7.84(d, $J= 15.6$ Hz, 1H), 7.94(dd, $J= 1.0, 3.8$ Hz, 1H), 7.99(dd, $J= 1.0, 4.9$ Hz, 1H), and 8.16(d, $J= 15.6$ Hz, 1H); ^{13}C NMR δ (in DMSO- d_6) 12.4, 55.3, 55.9, 94.8, 114.5, 117.0, 122.6, 124.8, 128.2, 128.9, 130.1,

132.0, 134.3, 136.4, 139.9, 142.7, 146.8, 160.2, 160.5, and 182.8; HR/MS calcd. for $C_{25}H_{24}O_4S$ (M+H)⁺ 421.1440, found 421.1425.

2.2. Clonogenic assay

The effect of SPP derivatives on the clonogenicity of HCT116 cells was determined as described previously [22]. Briefly, HCT116 colon cancer cells were seeded onto 24-well tissue culture plates (BD FalconTM; Becton Dickinson Immunocytometry Systems, San Jose, CA) at a density of 2×10^3 cells per well. After 24 h, the cells were treated with different concentrations of the compounds for 7 days and stained with 0.1% (w/v) crystal violet [27].

2.3. Cell viability assay

The effect of the compound SPP19 on cell viability was determined by using a Cell Counting Kit-8 (CCK-8; Dojindo Molecular Technologies, Gaithersburg, MD) in accordance with the manufacturer's instructions. Briefly, exponentially growing HCT116 cells (3×10^3 cells/sample) were treated with different concentrations of SPP19 (0, 10, 20, 50, and 100 μ M). After 24 h, CCK-8 solution containing the water-soluble tetrazolium salt WST-8 (2-(2-methoxy-4-nitrophenyl)-3-(4-nitrophenyl)-5-(2,4-disulfophenyl)-2H-tetrazolium, monosodium salt) was added and incubated for 1 h. The absorbance at 450 nm was measured by using an Emax Endpoint ELISA Microplate Reader (Molecular Devices, Sunnyvale, CA) [28].

2.4. Apoptosis assay by annexin V staining

HCT116 cells (1×10^6 cells/sample) were treated with different concentrations of compound SPP19 (0, 25, and 50 μM) for 24 h, fixed with 4% paraformaldehyde, and incubated with fluorescein isothiocyanate (FITC)-conjugated annexin V in accordance with the manufacturer's instructions (ChemoMetec). Propidium iodide (PI) staining was used to identify dead cells. The fluorescence intensities of FITC-annexin V-positive cells and PI-positive cells were analyzed by using a NucleoCounter NC-3000 instrument, as described previously [29].

2.5. Detection of intracellular ROS

HCT116 cells were incubated with 10 μM DCF-DA (Sigma-Aldrich) for 30 min and then exposed to 25 μM SPP19. After 1 and 12 h, the cells were collected and the fluorescence intensity was measured by using a FACSCalibur flow cytometer (Becton Dickinson Immunocytometry Systems, Jose, CA, USA), as described previously [17].

2.6. Immunoblot analysis

HCT116 cells were extracted in 20 mM pH 7.2 HEPES buffer containing 1% Triton X-100, 10% glycerol, 150 mM NaCl, 10 $\mu\text{g}/\text{mL}$ leupeptin, and 1 mM phenylmethylsulfonyl fluoride in an ice bath. The lysates were separated by 10% SDS-polyacrylamide gel electrophoresis and transferred to nitrocellulose membranes. The membranes were incubated with the corresponding primary antibodies and developed by using the enhanced chemiluminescence detection system (Amersham Pharmacia Biotech, Piscataway, NJ, USA) [30].

2.7. QSAR calculations

Three-dimensional quantitative structure-activity relationships (3D-QSARs) were performed by using an Intel Core 2 Quad Q6600 (2.4 GHz) Linux PC with Sybyl 7.3 software (Tripos, St. Louis, MO, USA). The experiment details are contained in a previously reported method [31].

2.8. Statistical Analysis

All statistical analyses were performed by using one-way analysis of variance (ANOVA) followed by a Kruskal-Wallis test using GraphPad InStat software (La Jolla, CA). P values of less than 0.05 indicated statistical significance [29].

3. Results and Discussion

Among the 26 SPP derivatives synthesized, 23 compounds are novel [25,26]—all except SPP **2**, **3**, and **7**. Therefore, one compound, (*E*)-3-(2-((*E*)-4-methoxystyryl)-4,6-dimethoxyphenyl)-1-(2-hydroxynaphthalen-1-yl)prop-2-en-1-one (SPP **13**) was selected for structural determination. In the ^1H NMR spectrum of SPP **13**, a total of 17 peaks were observed; 14 were found in the aromatic region. Of these, four peaks at 6.85, 6.96, 7.10, and 7.61 ppm were a doublet with a coupling constant of 16.1 Hz, indicating that they are from trans conformations of vicinal protons of alkene groups (CH=CH). The positions of the peaks were determined by using COSY and HMBC NMR experiments. For example, the peak at 7.61 ppm must be H- β , because of the correlation with both the carbonyl carbon (C=O, 197.7 ppm) and the quaternary carbon (C-1', 113.7 ppm) in the HMBC spectrum. In addition, a cross peak between the peaks at 7.10 ppm and 7.61 ppm was present in the COSY spectrum. Therefore, the peaks at 7.10 and 7.61 ppm were

assigned as H- α and H- β . The other two peaks at 6.85 and 6.96 ppm were H-7' and H-8', respectively, and assigned in a similar way. Two ^1H peaks at 6.57 and 6.79 ppm were a doublet with a coupling constant of 2.2 Hz, which is a typical $^4J_{\text{HH}}$ coupling constant. Therefore, they were assigned as H-3' and H-5', respectively. Two peaks at 7.14 and 6.91 ppm had 2H of integrated intensity, suggesting H-2''/6'' and H-3''/5'', respectively. The remaining peaks in the aromatic region were from the naphthalene moiety. The three peaks at approximately 3.80 ppm were methoxy protons. The positions of the methoxy protons were also determined by 2D NMR experiments, such as HMBC and NOESY. All methoxy protons showed long-range coupling with an adjacent quaternary carbon in the HMBC spectrum. For example, the ^1H peak at 3.87 ppm showing a singlet and 3H of integrated intensity was correlated with 160.7 ppm (C-2'), which indicated that the peak must be 2'-OCH₃. In addition, NOE cross peaks between the methoxy protons and the adjacent protons supported the positional determinations.

There are many methods to screen the anticancer effects of the compounds. The 26 SPP derivatives contain different substituents at two positions, but they have a common feature. Therefore, the clonogenic long-term survival assay was adapted for use here. Although this method requires a long experimental period, such as a minimum of 7 days, it is good for the discrimination of the cytotoxicity of compounds with similar structures. The inhibitory effects of the growth of HCT116 human colon cancer cells caused by different concentrations of the compounds synthesized are shown in Figure 2. The first clonogenic assay was performed at 0, 1, 5, 10, and 20 μM , and the second assay was at lower concentrations, such as 0, 0.1, 0.5, 1, and 5 μM . The clonogenic survival of the cancer cells was evaluated by using densitometry [32] and the half-maximal cancer cell growth inhibitory concentrations (GI_{50}) were determined by using

SigmaPlot software (SYSTAT, Chicago, IL). These values were between 3.41 and 91.42 μM , as listed in Table 1. The GI₅₀ values with error bars are graphed as shown in Suppl. Figure 1. The biological data for 3D-QSAR calculations were the negative logarithmic scales of the GI₅₀ values (pGI₅₀). To determine the 3D structures of the SPP derivatives tested here, the crystal structure of (*E*)-4,6-dimethoxy-2-(4-methoxystyryl)-3-methylbenzaldehyde was used as a template [33]. The 3D structures of all derivatives were determined based on the modification of this template structure. Comparative Molecular Field Analysis (CoMFA) and Comparative Molecular Similarity Indices Analysis (CoMSIA) were used for the 3D-QSAR calculations. The 26 derivatives were separated into the training set, used to build the QSAR model, and the test set, used to validate the model. Five derivatives (SPP **9**, **10**, **14**, **17**, and **24**) were selected arbitrarily and hierarchical clustering analysis was performed to confirm whether they belonged to the same structural group. As shown in Suppl. Figure 2, the five derivatives belonged to the separate groups. The derivatives contained in the training set were aligned to confirm whether they interacted with each other. As shown in Suppl. Figure 3, they were well aligned.

CoMFA calculations were iterated to find the best model able to elucidate the relationships between the structural properties of the SPP derivatives and their cytotoxicities obtained from the clonogenic long-term survival assay in HCT116 human colon cancer cells. Of the many CoMFA models, one model was chosen, which showed a good cross-validation correlation coefficient (0.503). In this CoMFA model, the non-cross-validated coefficient, optimal number of components, standard error estimation, and F values were 0.958, 5, 0.078, and 68.287, respectively. CoMFA provides information about steric and electrostatic field descriptors. In this CoMFA model, these descriptors contributed 64.4% and 35.6%, respectively. Using this

CoMFA model, the pGI_{50} values of the derivatives contained in the training set were calculated. As listed in Suppl. Table 1, the residuals between the experimental values of pGI_{50} and the values calculated using this CoMFA model were between 0.12% and 13.59%. Similarly, the residuals in the test set were between 7.18% and 28.79%. The experimental values of pGI_{50} were plotted against the pGI_{50} values predicted by this CoMFA model (Suppl. Figure 4). The plot indicated that this CoMFA model was reliable. To visualize the steric and electrostatic field descriptors calculated by this CoMFA model, contour maps were generated by using Sybyl software. SPP **19** is illustrated in the contour maps of CoMFA model as a template. In the steric field maps of CoMFA, yellow (14% contribution) and green (86% contribution) contours were observed in the second and fifth position of the pyridine structure, respectively (Figure 3A). The yellow contour indicates that the bulky group may decrease the biological activity. For example, the structures of SPP **5** and SPP **3** are identical, except for the substituents at C-2: SPP **5** has hydroxyl group instead of the H in SPP **3**, but the GI_{50} values were poorer. In contrast, green contours were observed mainly at the C-5 position, where the bulky group is thought to increase the biological activity. SPP **4**, with a bulky methoxy group at C-5, had a GI_{50} of 25.85 μM , which is more active than the values of SPP **5** (91.42 μM) and SPP **6** (27.72 μM). In addition, SPP **8** and SPP **9** have bulky groups of $-\text{NO}_2$ and $-\text{Br}$ at the C-5 position, respectively, which showed good GI_{50} values. The electrostatic field maps were displayed in Figure 3B. The blue (17% contribution) and red (83% contribution) contours indicate that electropositive and electronegative groups enhance the activity, respectively. The electropositive group at the second position increases the activity, such as the nitrogen atom of SPP **19**. Red contours were observed near C-3 and C-5, indicating that electronegative groups may increase the activity. SPP **18**, with

a furan ring that contained a negatively charged oxygen at the C-3 position, showed better activity than SPP **14** and SPP **16**, which contained the less negatively charged -NH and -S groups, respectively.

Similar to CoMFA calculations, CoMSIA calculations were performed using the same training set and the test set. Whereas CoMFA provides information about the steric and electrostatic field descriptors, CoMSIA provides information about the steric and electrostatic field descriptors, as well as hydrophobic interactions, hydrogen bond (H-bond) donors, and H-bond acceptor field descriptors. After many iterations of CoMSIA calculations, the model with a cross-validated coefficient of 0.626 was chosen. This model included three field descriptors, such as the steric, electrostatic, and H-bond donor descriptors, which contributed 7.4%, 55.8%, and 36.8%, respectively. Here, the non-cross-validated coefficient, the optimal number of components, standard error estimation, and *F* values were 0.954, 6, 0.085, and 48.154, respectively. The pGI_{50} values of the derivatives contained in the training set predicted by using this CoMSIA model are listed in Suppl. Table 1. The residuals between the experimental values of pGI_{50} and the predicted values were between 0.24% and 8.66%. Similarly, the residuals for the test set were between 16.49% and 30.70%. The experimental values of pGI_{50} were plotted versus the pGI_{50} values predicted using this CoMSIA model (Suppl. Figure 5), and the plot indicated that this CoMSIA model was considered reliable. The contour maps for CoMSIA were generated to visualize the results obtained from the CoMSIA model. The steric and electrostatic contours of the CoMSIA model (Suppl. Figure 6A, 6B) were similar to those of the CoMFA model. In the steric contour maps, two yellow contours at the C-4 and C-3' positions were newly observed; this may provide an explanation for why compounds with the methoxy group at C-4,

such as SPP **3**, SPP **5**, and SPP **22**, had poor activity. In contrast, a bulky group at C-3' may have a weaker effect on the activity. Although some of the SPP derivatives without a CH₃ group at the C-3' position showed better activities than the derivatives with a CH₃ group, the differences in GI₅₀ values between the derivatives were small. The contour maps for the H-bond donor of the CoMSIA model, illustrated with cyan and purple colors, indicate the H-bond donor-favored and -disfavored regions, respectively (Suppl. Figure 6C). Based on the H-bond donor contour maps of the CoMSIA model, the H-bond donor groups were favored near the C-4 and C-5 region. SPP **7**, with a hydroxyl group at the C-4 position, and SPP **25**, with a hydroxyl group at the C-5 position, showed good GI₅₀ values of 7.51 μM and 7.08 μM, respectively.

Based on the CoMFA and CoMSIA models, the pharmacophores of the SPP structures were elucidated, as shown in Figure 4. A bulky group was disfavored in the C-2 and C-4 positions, but favored at the C-5 position. In addition, electropositive groups, such as nitrogen or methoxy groups, are favored at the C-2 position and electronegative groups are favored at the C-3 and C-5 position. The presence of an H-bond donor group at C-4 and C-5 enhances the activity.

We selected SPP **19** for the evaluation of its cytotoxic effect. HCT116 cells in the exponential growth phase were treated with different concentrations of SPP **19** (0, 5, 10, 25, and 50 μM) for 24 h and the cell viability was measured. Treatment with >10 μM SPP **19** significantly reduced the viability of HCT116 cells (Figure 5). It has been reported that phosphatidylserine (PS) in the inner plasma membrane translocates to the outer membrane during apoptosis. As annexin V preferentially binds to PS [34], apoptotic cells can be identified by using the annexin V binding assay. To investigate whether SPP **19** triggers apoptosis, an annexin V staining assay was performed. HCT116 cells treated with SPP **19** (25 or 50 μM) for

24 h were incubated with fluorescein isothiocyanate (FITC)-conjugated annexin V (AV) and with propidium iodide (PI) to stain dead cells. The PI/AV double-negative populations (top panels, lower left quadrant in each cytogram) represent viable cells, whereas PI negative/AV positive populations (top panels, lower right quadrant) represent early apoptotic cells. PI/AV double-positive populations (top panels, upper right quadrant) are late apoptotic or dead cells. As shown in Figure 6A, the AV-positive populations increased from 8% (0 μ M) to 84% (25 μ M) and 90% (50 μ M) after SPP **19** treatment, which suggested that SPP **19** triggered apoptotic cell death in HCT116 cells. Caspases (cysteine-dependent aspartate-directed proteases) function as mediators of apoptosis [35]. To determine whether SPP **19** induced caspase activation, caspase activity was determined through the measurement of the cleavage of poly(ADP-ribose) polymerase (PARP), a well-known substrate for executioner caspases (e.g., caspase-3 and caspase-7), by using immunoblotting analysis. SPP **19** treatment increased the abundance of cleaved PARP in a time-dependent manner (Figure 6B). These data suggested that SPP **19** triggered apoptosis through a caspase-mediated pathway.

Many types of cancer cells are more sensitive to ROS than normal cells [36,37]; thus, ROS production is predicted to offer a valuable therapeutic approach to targeting cancer cells [38,39]. Given that ROS activates caspase in a variety of mammalian cells [40], we determined whether SPP **19** stimulated intracellular ROS production by using a H₂-2',7'-dichlorofluorescein diacetate (DCF-DA) probe. We found that SPP **19** treatment led to detectable ROS accumulation after 1 h, with this level maintained until 12 h (Figure 7A). To further evaluate the effect of SPP **19** on ROS production, intracellular ROS was visualized by using fluorescence microscopy (Figure 7B). To determine whether SPP **19**-induced ROS production was functionally associated

with the induction of apoptosis, HCT116 cells were pretreated with 2 mM *N*-acetyl cysteine (NAC), a thiol-containing ROS scavenger. SPP **19**-induced PARP cleavage was substantially reduced by pretreatment with NAC (Figure 7C). These results suggested that SPP **19**-induced apoptosis occurred through a ROS-dependent caspase-mediated pathway.

4. Conclusion

To find compounds generating ROS, 26 SPP derivatives designed to contain a Michael acceptor, were synthesized. Of these 26 derivatives, 23 were novel. The derivatives were identified by using NMR spectroscopy and HR/MS. Their cytotoxicity to HCT116 colon cancer cells were measured by using a clonogenic long-term survival assay. Their half-maximal cell growth inhibitory effect was between 3.41 and 91.42 μ M. The compound with the strongest cytotoxicity was examined by using a DCF-DA probe to confirm whether it generated ROS. As expected, the title compound, (*E*)-3-(2-((*E*)-4-methoxystyryl)-4,6-dimethoxyphenyl)-1-(pyridin-2-yl)prop-2-en-1-one, caused an accumulation of ROS at 1 h. In addition, intracellular ROS determined by the title compound was confirmed by using fluorescence microscopy. ROS generation by the title compound was linked to the induction of apoptosis, which was confirmed by pretreatment with *N*-acetyl cysteine. The search for ROS-generating compounds is linked to the discovery of new chemotherapeutic agents. Therefore, the structural conditions that show better cytotoxicity were derived based on CoMFA and CoMSIA. Although the presence of a bulky group at the C-2 and C-4 positions is not favored, it is favored at the C-5 position. In addition, electropositive groups, such as nitrogen or methoxy groups, are favored at the C-2 position and electronegative groups

are favored at the C-3 and C-5 positions. The presence of the H-bond donor group at C-4 and C-5 enhances cytotoxicity. The design of the 26 compounds containing a Michael acceptor synthesized in this study were based on the combination of chalcone and resveratrol. Their cytotoxicities were not improved greatly compared with those caused by known chalcone and resveratrol derivatives; however, 23 compounds synthesized here were novel and one was confirmed to result in ROS generation. These findings can assist in the design of novel compounds with a combination of the structures of chalcone and resveratrol for use as chemotherapeutic agents.

Acknowledgments

This study was supported by the Basic Science Research Program (NRF-2016R1D1A1A09919045). SY Shin was supported by the KU Research Professor Program of Konkuk University.

References

- [1] A.A. Alfadda, R.M. Sallam, *J Biomed Biotechnol.* 2012 (2012) 936486.
- [2] L.O. Klotz, *Biol Chem.* 383 (2002) 443–456.
- [3] J.F. Turrens, *J Physiology.* 552 (Pt 2) (2003) 335–344.
- [4] F. Muller, *J Am Aging Assoc.* 23 (2000) 227-53.
- [5] J.T. Hancock, R. Desikan, S.J. Neill, *Biochem Biomed Aspects Oxi Mod.* 29 (2001) 345-350.
- [6] J. Boonstra, J.A. Post, *Gene.* 337 (2004) 1–13.

- [7] G. Perry, A.K. Raina, A. Nunomura, T. Wataya, L.M. Sayre, M.A. Smith, *Free Radic Biol Med.* 28 (2000) 831–834.
- [8] P. Møller, N.R. Jacobsen, J.K. Folkmann, P.H. Danielsen, L. Mikkelsen, J.G. Hemmingsen, L.K. Vesterdal, L. Forchhammer, H. Wallin, S. Loft, *Free Radic Res.* 44 (2010) 1-46.
- [9] S. Galadari, A. Rahman, S. Pallichankandy, F. Thayyullathil, *Free Radic Biol Med.* 104 (2017) 144-164.
- [10] D. Trachootham, J. Alexandre, P. Huang, *Nature Rev Drug Discovery.* 8 (2009) 579–591.
- [11] D.J. Adams, Z.V. Boskovic, J.R. Theriault, A.J. Wang, A.M. Stern, B.K. Wagner, A.F. Shamji, S.L. Schreiber, *ACS Chem Biol.* 8 (2013) 923-929.
- [12] L. Raj, T. Ide, A.U. Gurkar, M. Foley, M. Schenone, X. Li, N.J. Tolliday, T.R. Golub, S.A. Carr, A.F. Shamji, A.M. Stern, A. Mandinova, S.L. Schreiber, S.W. Lee, *Nature.* 475 (2011)231-234.
- [13] A.T. Dinkova-Kostova, M.A. Massiah, R.E. Bozak, R.J. Hicks, P. Talalay, *Proc Natl Acad Sci U S A.* 98 (2001) 3404–3409.
- [14] C.P. Schröder, A.K. Godwin, P.J. O'Dwyer, K.D. Tew, T.C. Hamilton, R.F. Ozols, *Cancer Invest.* 14 (1996) 158-168.
- [15] N. Couto, N. Malys, S.J. Gaskell, J. Barber, *J Proteome Res.* 12 (2013) 2885-2894.
- [16] S.Y. Shin, J.M. Lee, M.S. Lee, D. Koh, H. Jung, Y. Lim, Y.H. Lee, *Clin Cancer Res.* 20 (2014) 4302-4313.
- [17] D.H. Lee, J.Y. Jung, D. Koh, Y. Lim, Y.H. Lee, S.Y. Shin, *Cancer Lett.* 372 (2016) 1-9.
- [18] D.Y. Lee, D.H. Lee, J.Y. Jung, D. Koh, G.S. Kim, Y.S. Ahn, Y.H. Lee, Y. Lim, S.Y. Shin, *Bioorg Med Chem Lett.* 26 (2016) 203-208.

- [19] S.Y. Shin, J.H. Kim, H. Yoon, Y.K. Choi, D. Koh, Y. Lim, Y.H. Lee *J Agric Food Chem.* 61 (2013) 12588-12597.
- [20] H. Dai, H.B. Deng, Y.H. Wang, J.J. Guo, *Oncol Lett.* 16 (2018) 1579-1583.
- [21] M. Elshaer, Y. Chen, X.J. Wang, X. Tang, *Life Sci.* 207 (2018) 340-349.
- [22] N.A. Franken, H.M. Rodermond, J. Stap, J. Haveman, C. van Bree, *Nat Protoc.* 1 (2006) 2315-2319.
- [23] H. Jung, S. Ahn, Y. Jung, D. Koh, Y. Lim, *Magn Reson Chem.* 54 (2016) 246-251.
- [24] S. Ahn, S.Y. Shin, Y. Jung, H. Jung, B.S. Kim, D. Koh, Y. Lim, *Magn Reson Chem.* 54 (2016) 382-390.
- [25] B.F. Ruan, X. Lu, J.F. Tang, Y. Wei, X.L. Wang, Y.B. Zhang, L.S. Wang, H.L. Zhu, *Bioorg Med Chem.* 19 (2011) 2688-2695.
- [26] F.Z. Shenqing, CN patent. 102093191 (2011) A 20110615.
- [27] K.Y. Jung, J. Park, Y.S. Han, Y.H. Lee, S.Y. Shin, Y. Lim, *Bioorg Med Chem.* 25 (2017) 397-407.
- [28] S.Y. Shin, S. Ahn, H. Yoon, H. Jung, Y. Jung, D. Koh, Y.H. Lee, Y. Lim, *Bioorg Med Chem Lett.* 26 (2016) 4301-4309.
- [29] Y. Jung, S.Y. Shin, Y. Yong, H. Jung, S. Ahn, Y.H. Lee, Y. Lim, *Chem Biol Drug Des.* 85 (2015) 574-585.
- [30] J.M. Lee, M.S. Lee, D. Koh, Y.H. Lee, Y. Lim, S.Y. Shin, *Cancer Lett.* 354 (2014) 348-354.
- [31] Y. Lee, B.S. Kim, S. Ahn, D. Koh, Y.H. Lee, S.Y. Shin, Y. Lim, *Bioorg Chem.* 68 (2016) 166-176.

- [32] B.S. Kim, S.Y. Shin, S. Ahn, D. Koh, Y.H. Lee, Y. Lim, *Bioorg Med Chem.* 25 (2017) 5423-5432.
- [33] S. Ahn, Y. Lim, D. Koh, *Acta Crystallogr E Crystallogr Commun.* E71 (2015) o771.
- [34] H.A. Andree, C.P. Reutelingsperger, R. Hauptmann, H.C. Hemker, W.T. Hermens, G.M. Willems, *J Biol Chem.* 265 (1990) 4923-4928.
- [35] D.R. McIlwain, T. Berger, T.W. Mak, *Cold Spring Harb Perspect Biol.* 5 (2013) a008656.
- [36] B. Rigas, Y. Sun, *Br J Cancer.* 98 (2008) 1157-1160.
- [37] P.T. Schumacker, *Cancer Cell.* 10 (2006) 175-176.
- [38] L. Raj, T. Ide, A.U. Gurkar, M. Foley, M. Schenone, X. Li, N.J. Tolliday, T.R. Golub, S.A. Carr, A.F. Shamji, A.M. Stern, A. Mandinova, S.L. Schreiber, S.W. Lee, *Nature.* 475 (2011) 231-234.
- [39] D.J. Adams, M. Dai, G. Pellegrino, B.K. Wagner, A.M. Stern, A.F. Shamji, S.L. Schreiber, *Proc Natl Acad Sci U S A.* 109 (2012) 15115-15120.
- [40] B.M. Kim, A.B. Rode, E.J. Han, I.S. Hong, S.H. Hong, *Apoptosis.* 17 (2012) 200-216.

Figure legends

Figure 1. The structures of (A) (*E*)-3-(3,5-dimethoxyphenyl)-1-(2-methoxyphenyl)prop-2-en-1-one containing a Michael acceptor, (B) 1-aryl-(3-(2-styryl)phenyl)prop-2-en-1-ones in which the square and ellipse denote the chalcone and resveratrol skeletons, respectively; (C) chalcone, and (D) resveratrol.

Figure 2. The inhibitory effects on the growth of HCT116 human colon cancer cells caused by different concentrations of the synthesized compounds.

Figure 3. CoMFA contour maps. (A) Steric field contours of CoMFA (yellow, bulky group disfavored; and green, bulky group favored). (B) Electrostatic field contours (blue, electropositive group favored; and red, electronegative group favored).

Figure 4. The structural conditions that elicit more toxic 1-aryl-(3-(2-styryl)phenyl)prop-2-en-1-one derivatives to the HCT116 human colon cancer cell line.

Figure 5. Effect of SPP **19** on the cytotoxicity of HCT116 cells. HCT116 cells (1×10^5 cells/sample) were treated with different concentrations of SPP **19** (0, 5, 10, 25, and 50 μM). After 24 h, the cell viability was measured by using the Cell Counting Kit-8. The data shown represent the mean \pm S.D. NS, not significant; *, $p < 0.01$; **, $p < 0.001$ by Dunnett's multiple comparison test.

Figure 6. Effect of SPP **19** on the induction of apoptosis. (A) HCT116 cells were treated with SPP **19** (0, 25, and 50 μM) for 24 h, followed by staining with annexin V-FITC and propidium iodide (PI). The percentage of annexin V and PI-stained cells was measured by flow cytometry. Scatter plots (top panels) show the FITC-annexin V versus PI staining intensity. Histograms

(bottom panels) show the FITC-annexin V staining intensity of the cell population (%). (B) HCT116 cells were treated with 25 μ M SPP **19** for between 0 and 24 h, and whole cell lysates were prepared and subjected to immunoblotting analysis for PARP; GAPDH was monitored as an internal control to show equal protein loading.

Figure 7. Effect of SPP **19** on ROS production. (A and B) HCT116 cells were incubated with 10 μ M DCF-DA for 60 min, followed by the addition of vehicle (DMSO) or 25 μ M SPP **19** for 1 and 12 h. The fluorescence was measured by using flow cytometry (A) and fluorescence microscopy (B). Scale bars = 100 μ m. (C) HCT116 cells were pretreated with NAC for 30 min, followed by the addition of the vehicle (DMSO) or 25 μ M SPP **19** for 12 h. Whole cell lysates were prepared and subjected to immunoblotting for PARP; GAPDH was monitored as an internal control to show equal protein loading.

Scheme 1. The synthetic procedures of 1-aryl-(3-(2-styryl)phenyl)prop-2-en-1-ones.

Table legend

Table 1. Names and structures of the 26 derivatives of 1-aryl-(3-(2-styryl)phenyl)prop-2-en-1-ones and their half-maximal cell growth inhibitory activities (GI_{50} values).

Suppl. Table 1. The negative logarithmic scale of the experimental half-maximal cell growth inhibitory concentration (pGI_{50}) data and pGI_{50} values predicted by using the CoMFA and CoMSIA models, and their residuals. * denotes the test set.

Suppl. Figure 1. A graph of the GI_{50} values with error bars.

Suppl. Figure 2. Hierarchical clustering tree; the test set is colored red.

Suppl. Figure 3. Alignments of the SPP derivatives used for the training set.

Suppl. Figure 4. A plot of experimental data against values predicted by using CoMFA, where diamonds and squares denote the training and test sets, respectively.

Suppl. Figure 5. A plot of experimental data against values predicted by using CoMSIA, where diamonds and squares denote the training and test sets, respectively.

Suppl. Figure 6. CoMSIA contour maps. (A) Steric field contours (green, more bulky substituents favored) and yellow (less bulky substituents favored). (B) Electrostatic field contours (red, electronegative substituents favored; and blue, electropositive substituents favored). (C) H-bond donor field contours (cyan, H-bond donor favored; and purple, H-bond donor disfavored).

Figure 1

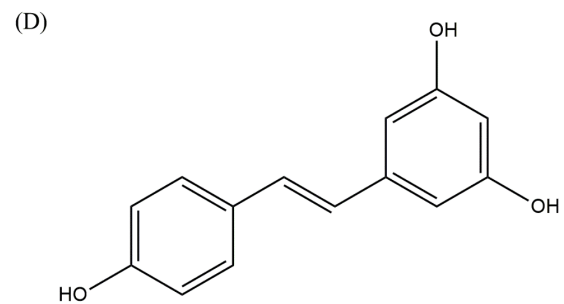
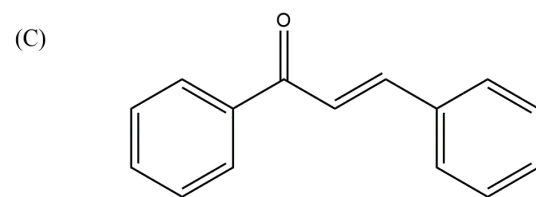
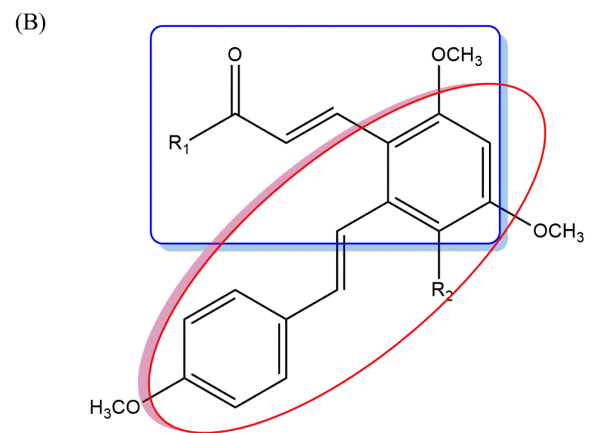
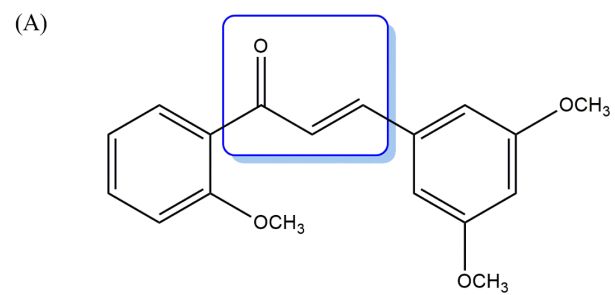


Figure 2

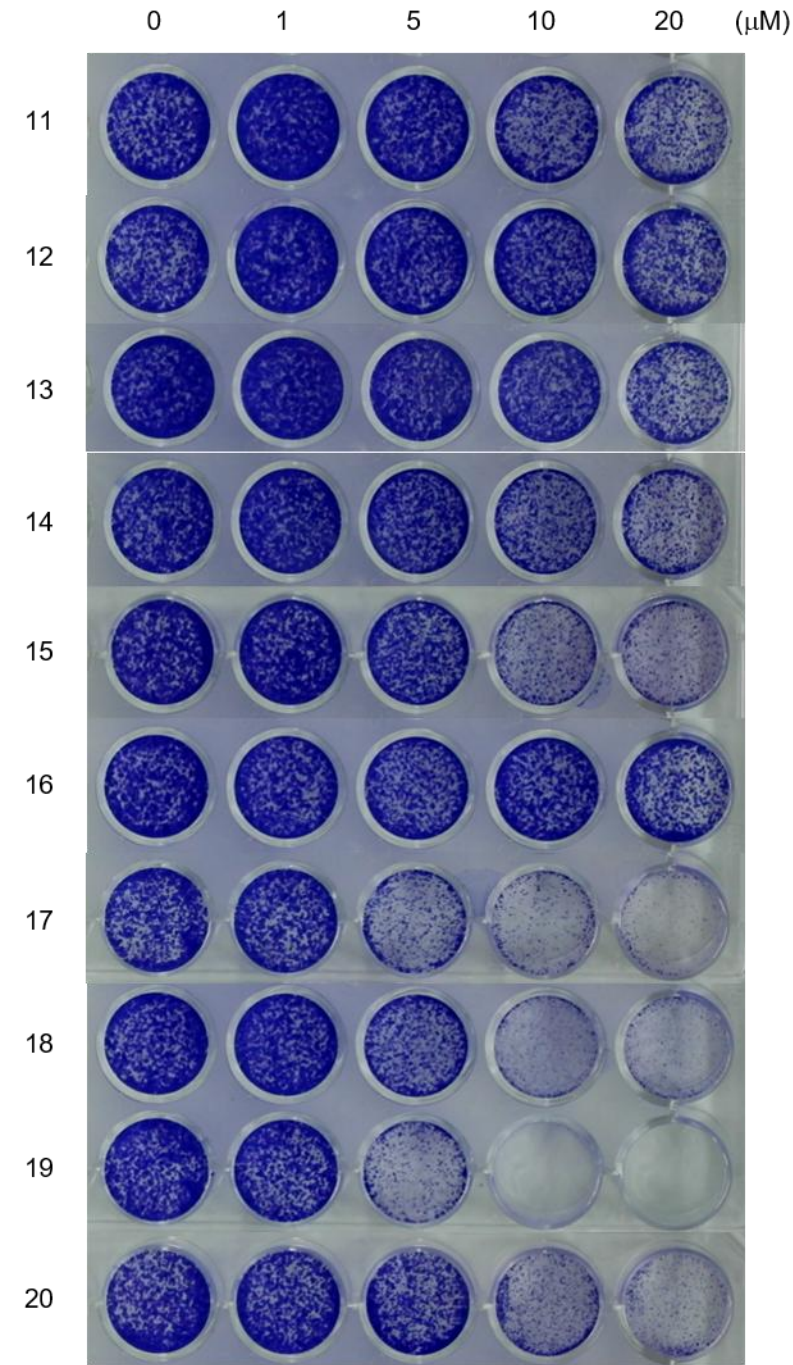
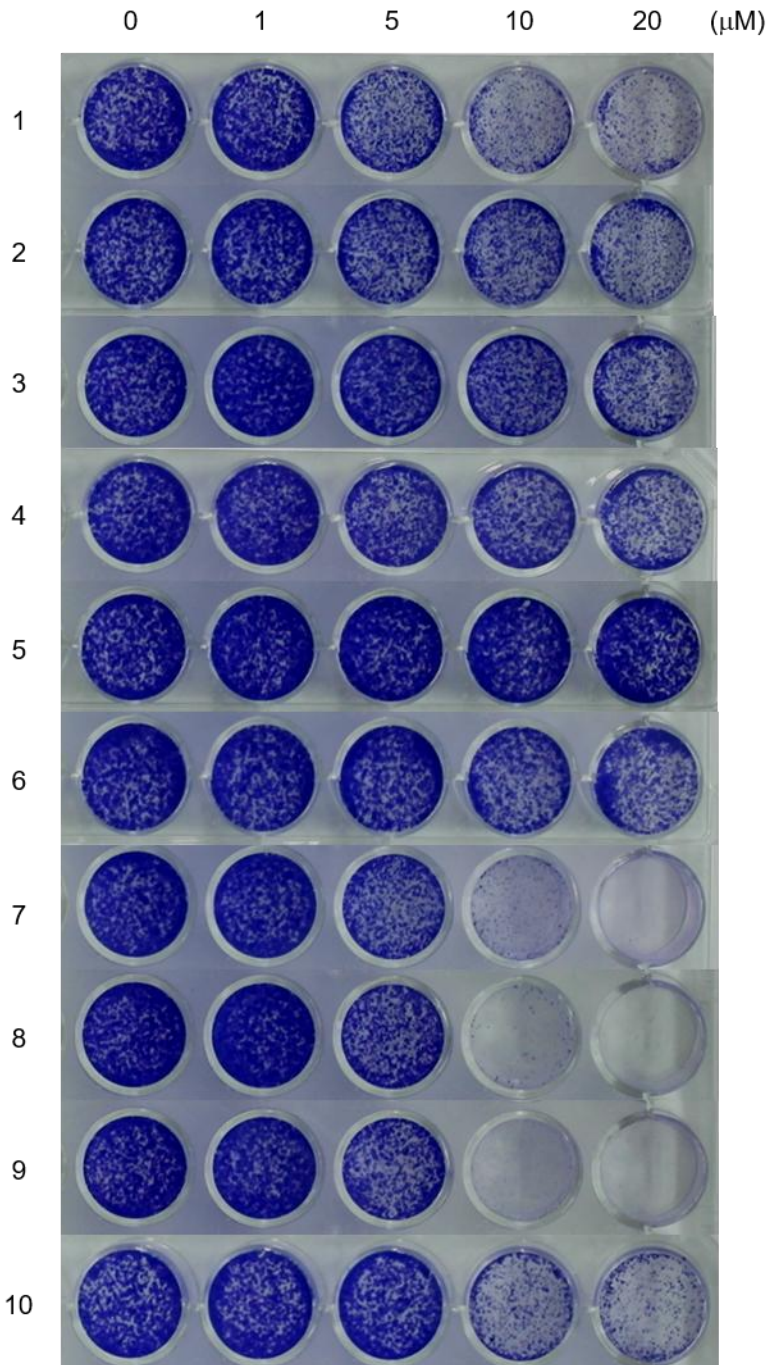


Figure 2 continued

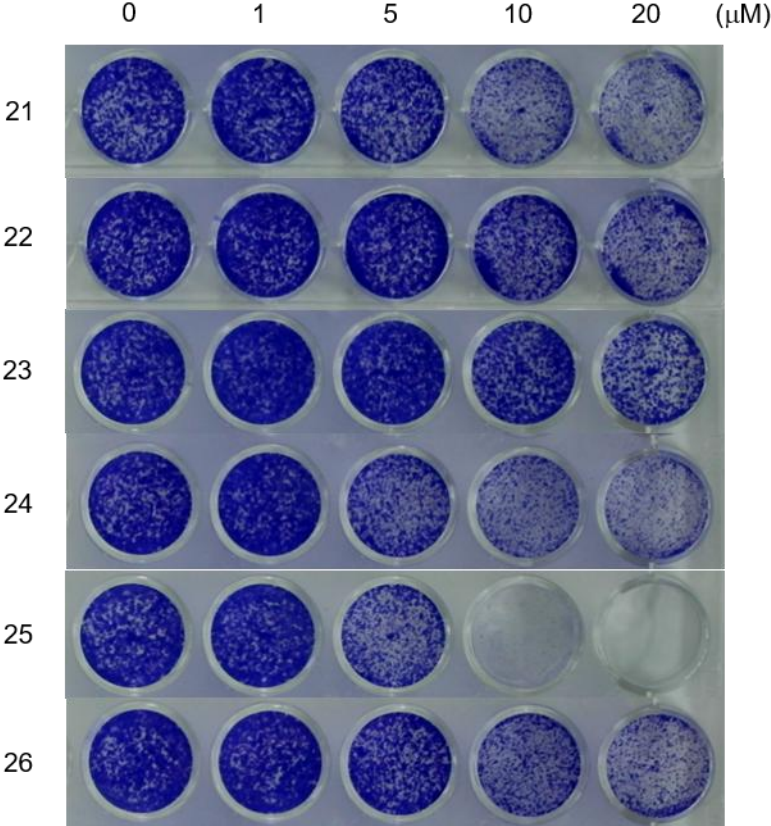
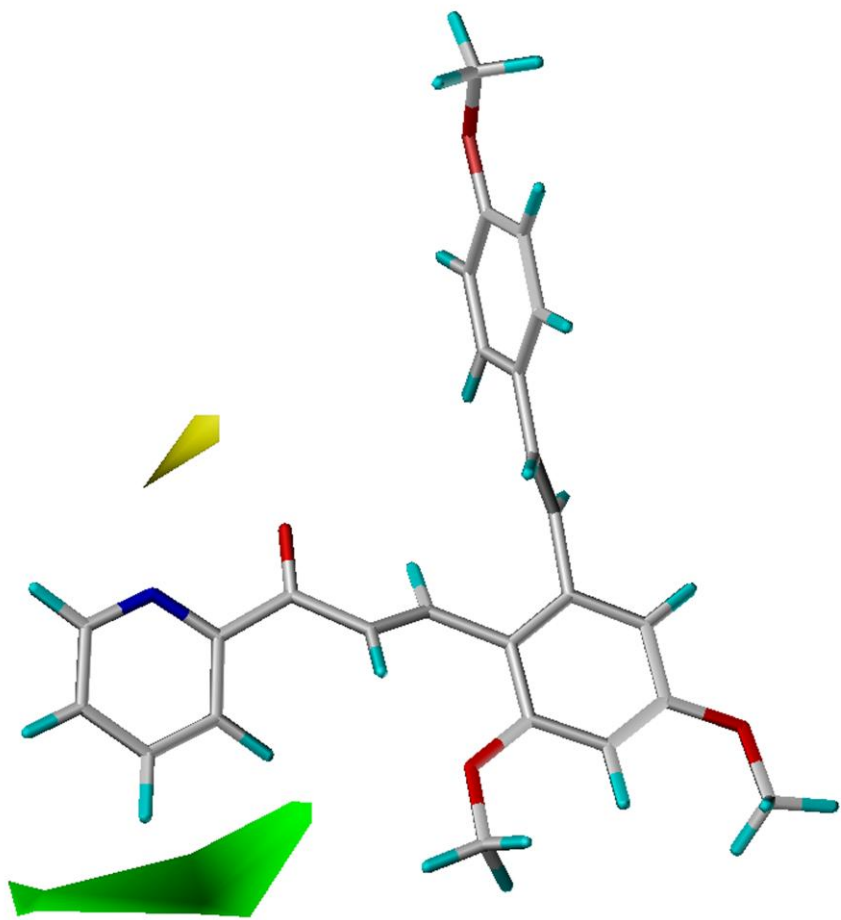


Figure 3

A



B

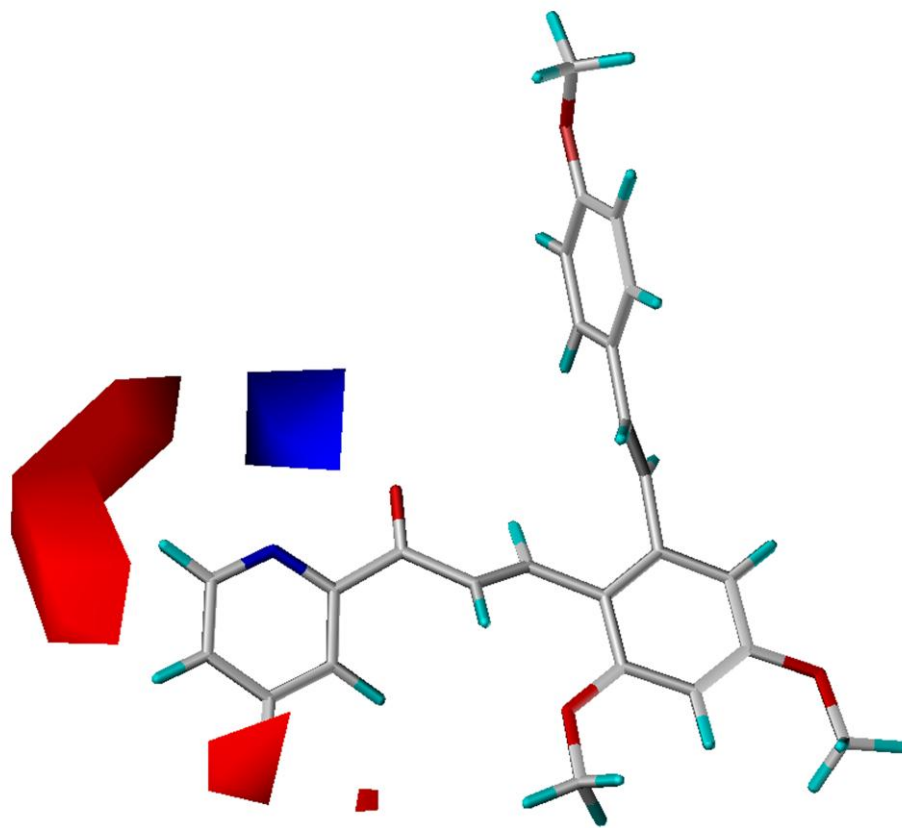


Figure 4

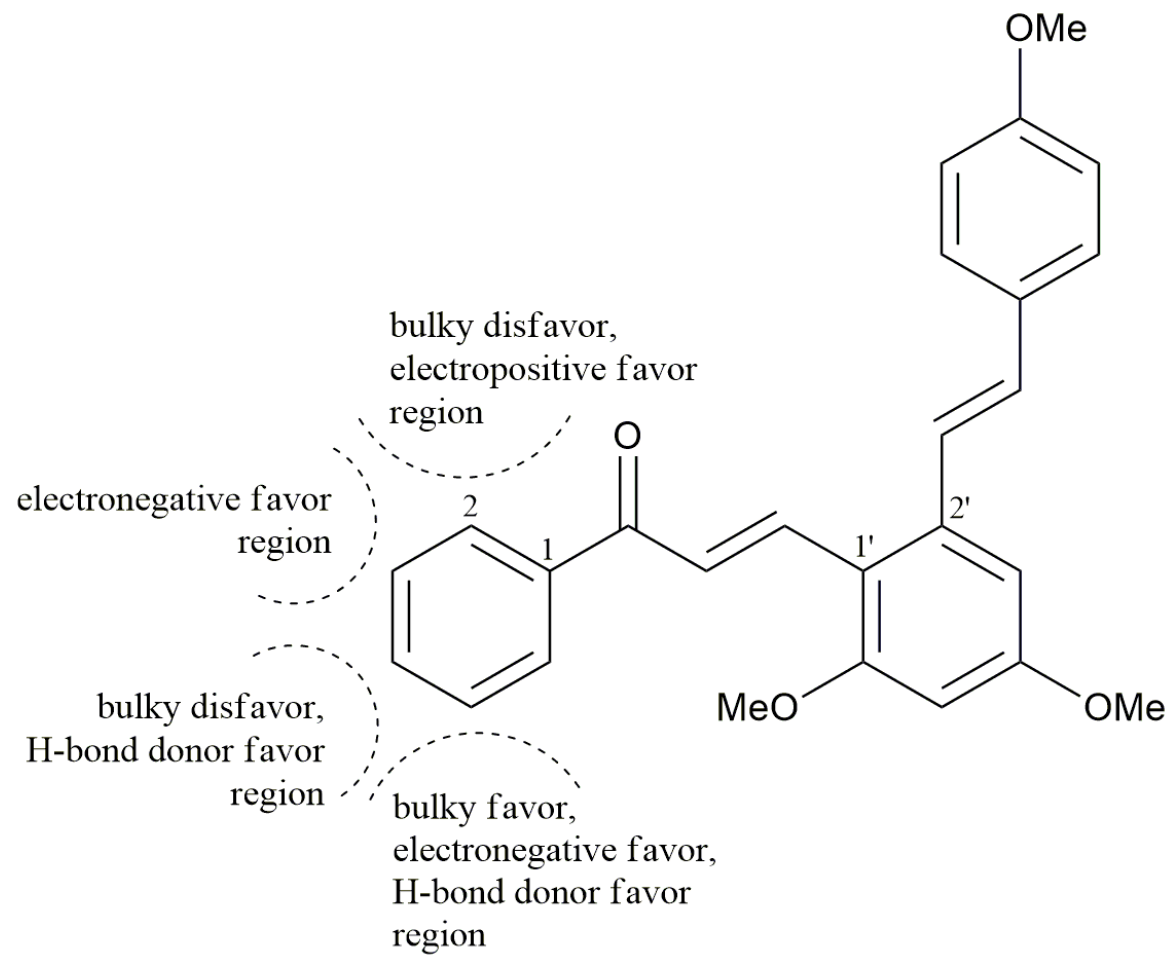


Figure 5

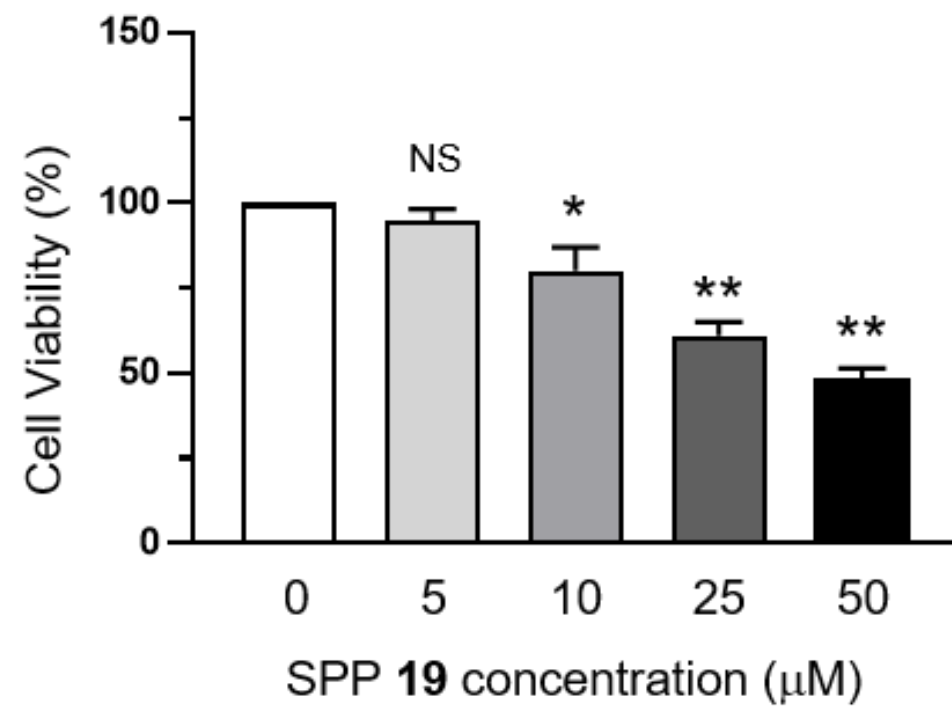


Figure 6

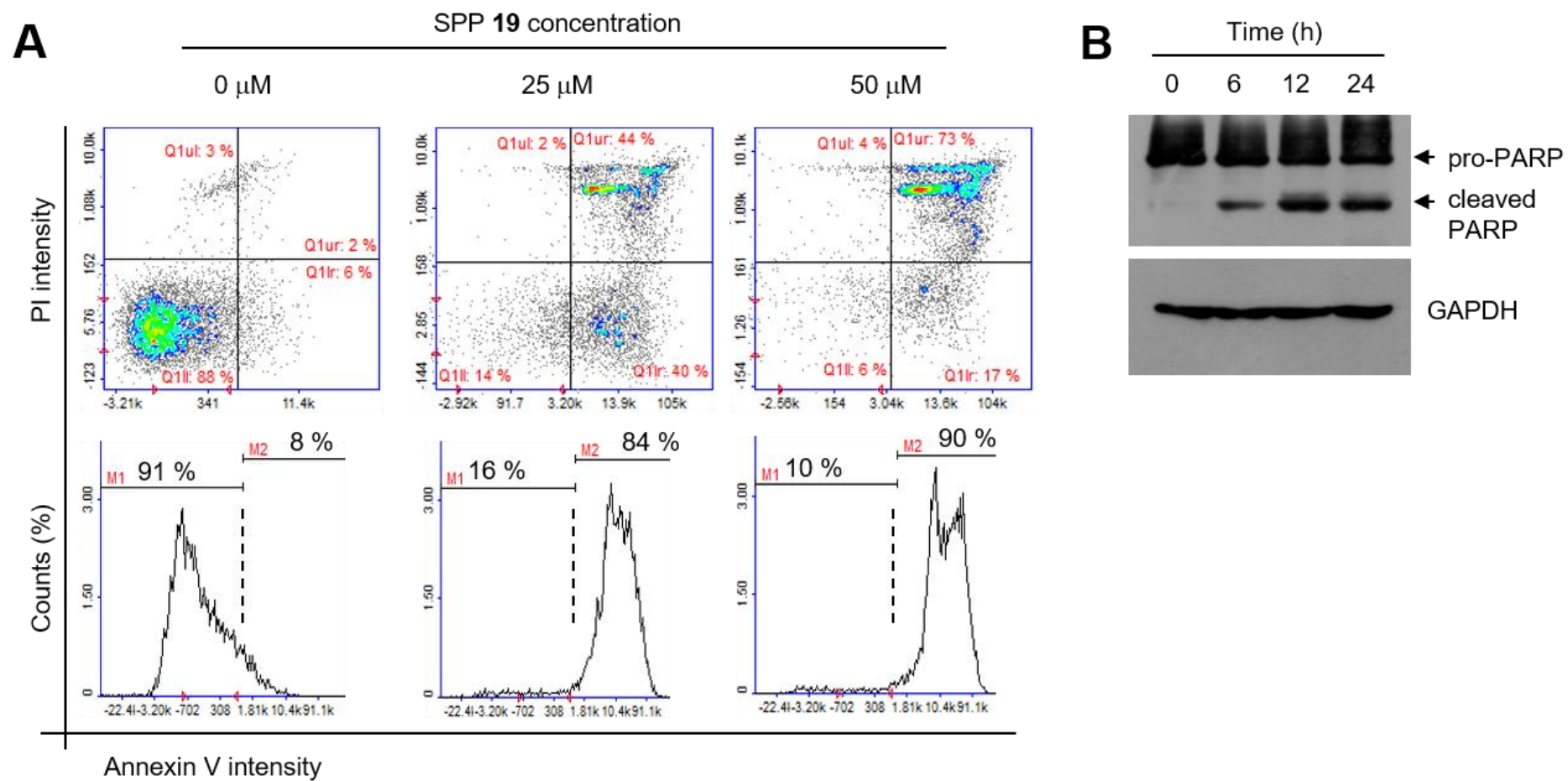
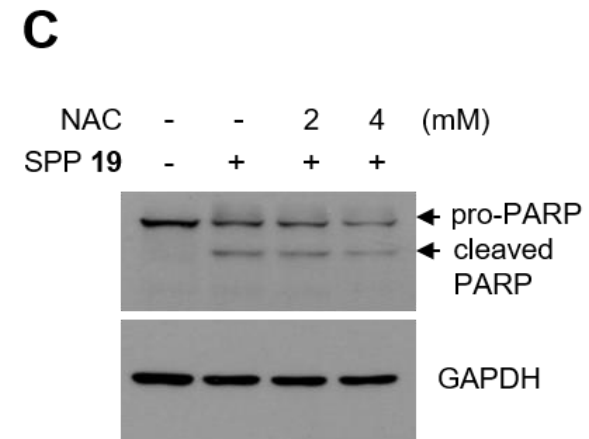
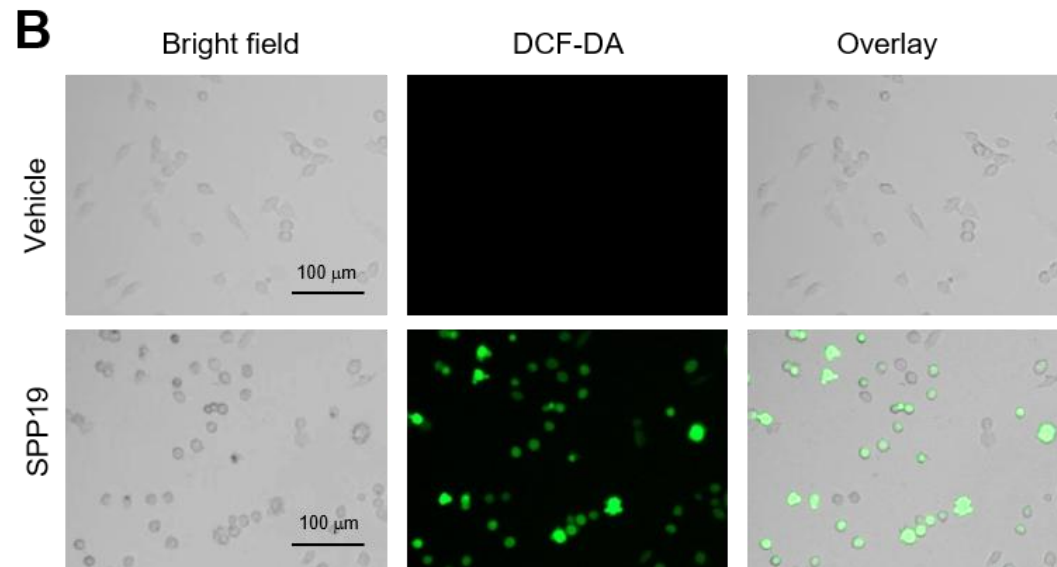
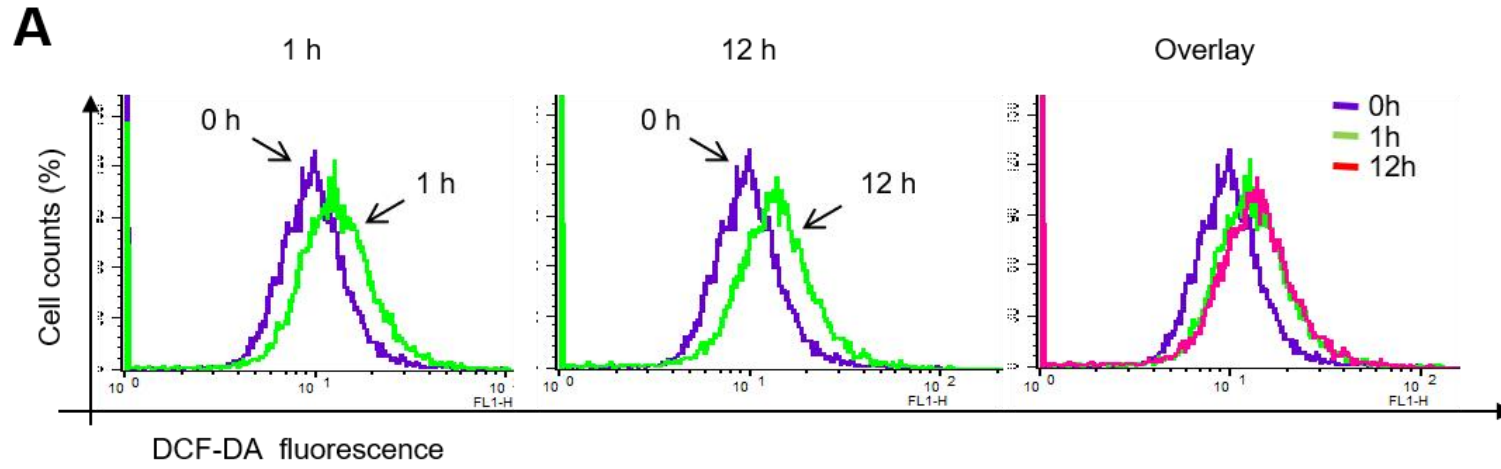


Figure 7



Scheme 1

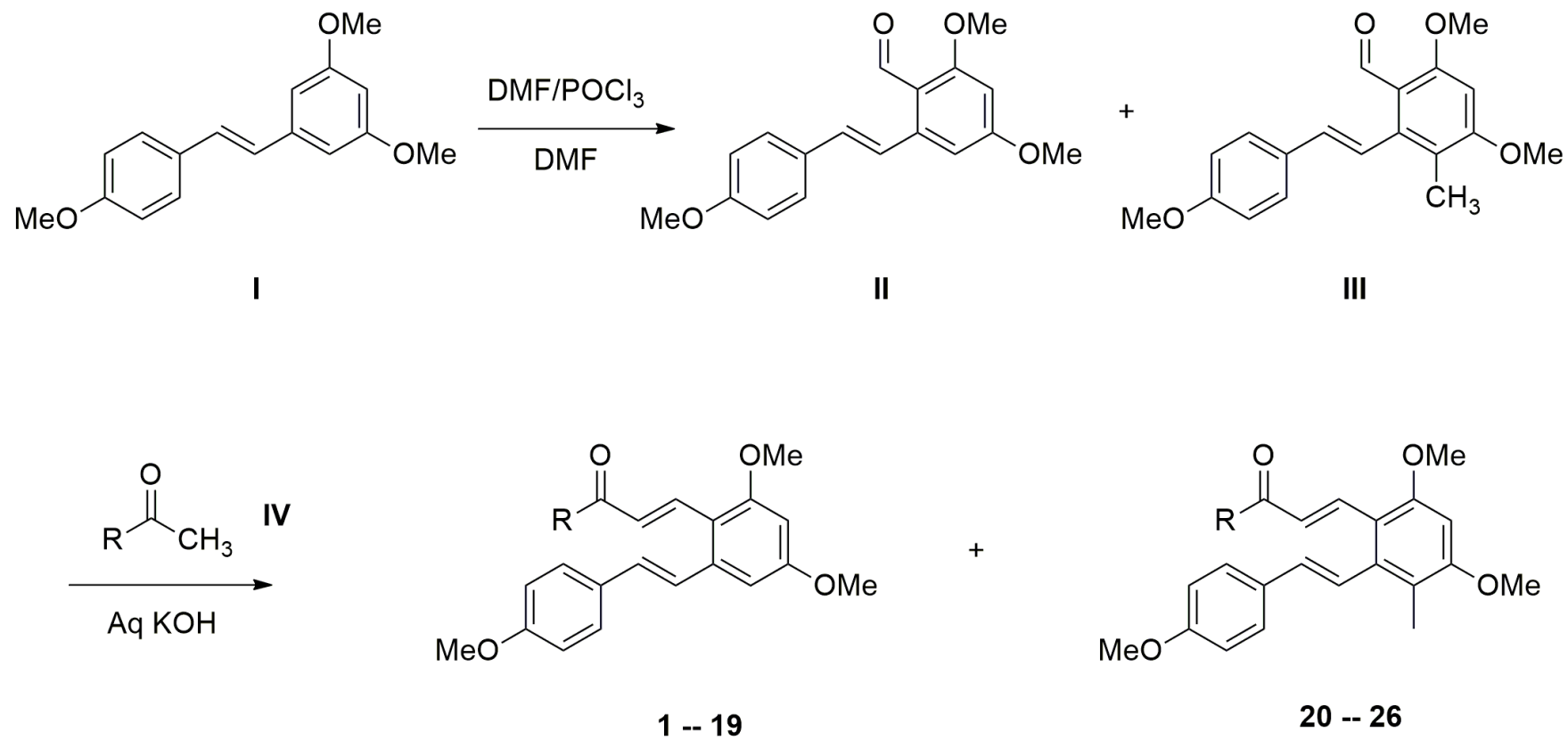
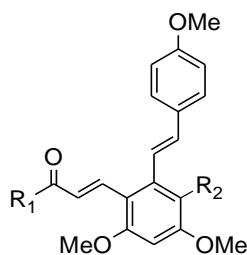
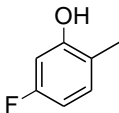
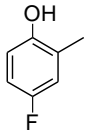
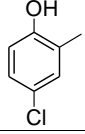
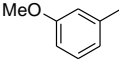
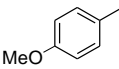
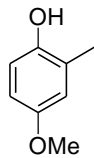
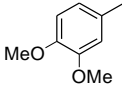
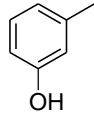


Table 1. Names and structures of 26 1-aryl-(3-(2-styryl)phenyl)prop-2-en-1-ones, and their half-maximal cell growth inhibitory activities (GI_{50}).

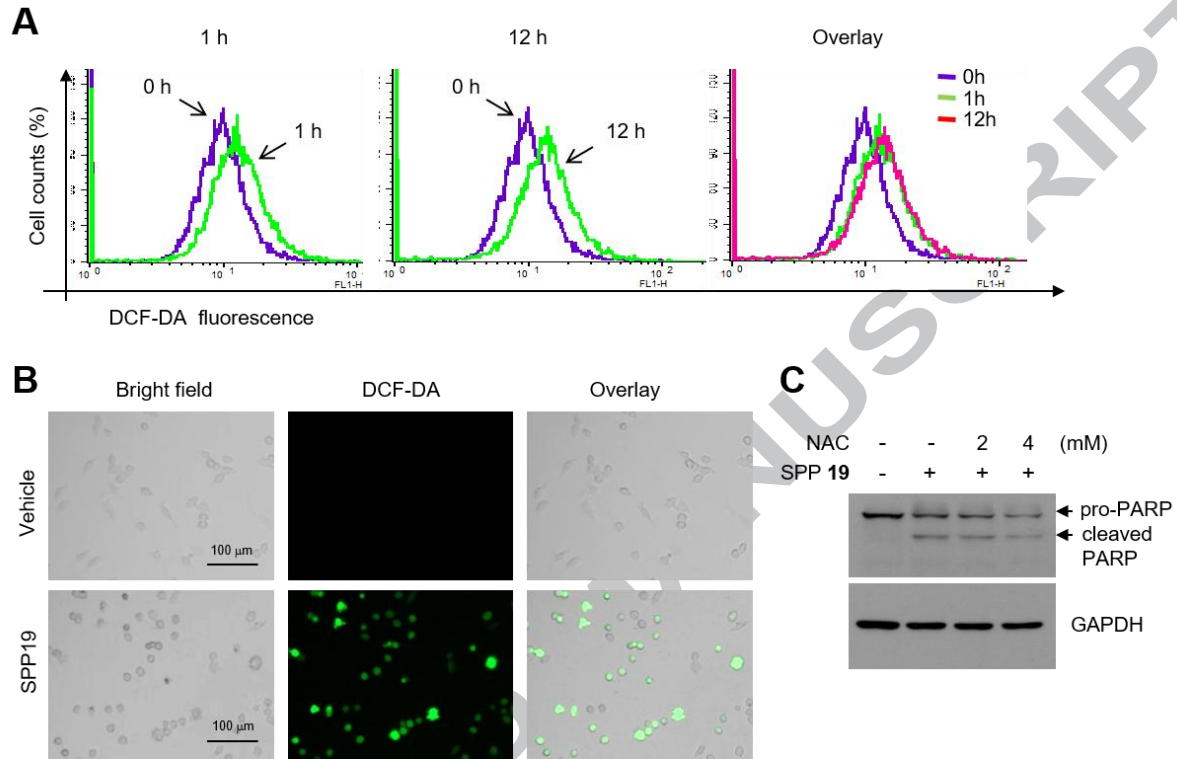


Derivative	Name	R ₁	R ₂	GI ₅₀ (μM)
1	(<i>E</i>)-3-(2-((<i>E</i>)-4-methoxystyryl)-4,6-dimethoxyphenyl)-1-(2-methoxyphenyl)prop-2-en-1-one		H	11.48
2	(<i>E</i>)-3-(2-((<i>E</i>)-4-methoxystyryl)-4,6-dimethoxyphenyl)-1-(3-methoxyphenyl)prop-2-en-1-one		H	24.91
3	(<i>E</i>)-3-(2-((<i>E</i>)-4-methoxystyryl)-4,6-dimethoxyphenyl)-1-(4-methoxyphenyl)prop-2-en-1-one		H	36.33
4	(<i>E</i>)-3-(2-((<i>E</i>)-4-methoxystyryl)-4,6-dimethoxyphenyl)-1-(2-hydroxy-5-methoxyphenyl)prop-2-en-1-one		H	25.85
5	(<i>E</i>)-3-(2-((<i>E</i>)-4-methoxystyryl)-4,6-dimethoxyphenyl)-1-(2-hydroxy-4-methoxyphenyl)prop-2-en-1-one		H	91.42
6	(<i>E</i>)-3-(2-((<i>E</i>)-4-methoxystyryl)-4,6-dimethoxyphenyl)-1-(2-hydroxyphenyl)prop-2-en-1-one		H	27.72
7	(<i>E</i>)-3-(2-((<i>E</i>)-4-methoxystyryl)-4,6-dimethoxyphenyl)-1-(4-hydroxyphenyl)prop-2-en-1-one		H	7.51
8	(<i>E</i>)-3-(2-((<i>E</i>)-4-methoxystyryl)-4,6-dimethoxyphenyl)-1-(2-hydroxy-5-nitrophenyl)prop-2-en-1-one		H	7.36
9	(<i>E</i>)-3-(2-((<i>E</i>)-4-methoxystyryl)-4,6-dimethoxyphenyl)-1-(5-bromo-2-hydroxyphenyl)prop-2-en-1-one		H	6.95

10	(<i>E</i>)-3-(2-((<i>E</i>)-4-methoxystyryl)-4,6-dimethoxyphenyl)-1-(4-fluoro-2-hydroxyphenyl)prop-2-en-1-one		H	12.78
11	(<i>E</i>)-3-(2-((<i>E</i>)-4-methoxystyryl)-4,6-dimethoxyphenyl)-1-(5-fluoro-2-hydroxyphenyl)prop-2-en-1-one		H	29.17
12	(<i>E</i>)-3-(2-((<i>E</i>)-4-methoxystyryl)-4,6-dimethoxyphenyl)-1-(5-chloro-2-hydroxyphenyl)prop-2-en-1-one		H	38.77
13	(<i>E</i>)-3-(2-((<i>E</i>)-4-methoxystyryl)-4,6-dimethoxyphenyl)-1-(2-hydroxynaphthalen-1-yl)prop-2-en-1-one		H	28.14
14	(<i>E</i>)-3-(2-((<i>E</i>)-4-methoxystyryl)-4,6-dimethoxyphenyl)-1-(thiophen-2-yl)prop-2-en-1-one		H	27.48
15	(<i>E</i>)-3-(2-((<i>E</i>)-4-methoxystyryl)-4,6-dimethoxyphenyl)-1-(thiophen-3-yl)prop-2-en-1-one		H	15.86
16	(<i>E</i>)-3-(2-((<i>E</i>)-4-methoxystyryl)-4,6-dimethoxyphenyl)-1-(1 <i>H</i> -pyrrol-2-yl)prop-2-en-1-one		H	34.49
17	(<i>E</i>)-3-(2-((<i>E</i>)-4-methoxystyryl)-4,6-dimethoxyphenyl)-1-(thiazol-2-yl)prop-2-en-1-one		H	6.91
18	(<i>E</i>)-3-(2-((<i>E</i>)-4-methoxystyryl)-4,6-dimethoxyphenyl)-1-(furan-2-yl)prop-2-en-1-one		H	9.22
19	(<i>E</i>)-3-(2-((<i>E</i>)-4-methoxystyryl)-4,6-dimethoxyphenyl)-1-(pyridin-2-yl)prop-2-en-1-one		H	3.41
20	(<i>E</i>)-3-(2-((<i>E</i>)-4-methoxystyryl)-4,6-dimethoxy-3-methylphenyl)-1-(2-methoxyphenyl)prop-2-en-1-one		CH ₃	13.11
21	(<i>E</i>)-3-(2-((<i>E</i>)-4-methoxystyryl)-4,6-dimethoxy-3-methylphenyl)-1-(3-methoxyphenyl)prop-2-en-1-one		CH ₃	22.39
22	(<i>E</i>)-3-(2-((<i>E</i>)-4-methoxystyryl)-4,6-dimethoxy-3-methylphenyl)-1-(4-methoxyphenyl)prop-2-en-1-one		CH ₃	31.27

23	(<i>E</i>)-3-(2-((<i>E</i>)-4-methoxystyryl)-4,6-dimethoxy-3-methylphenyl)-1-(2-hydroxy-5-methoxyphenyl)prop-2-en-1-one		CH ₃	29.83
24	(<i>E</i>)-3-(2-((<i>E</i>)-4-methoxystyryl)-4,6-dimethoxy-3-methylphenyl)-1-(3,4-dimethoxyphenyl)prop-2-en-1-one		CH ₃	13.70
25	(<i>E</i>)-3-(2-((<i>E</i>)-4-methoxystyryl)-4,6-dimethoxy-3-methylphenyl)-1-(3-hydroxyphenyl)prop-2-en-1-one		CH ₃	7.08
26	(<i>E</i>)-3-(2-((<i>E</i>)-4-methoxystyryl)-4,6-dimethoxy-3-methylphenyl)-1-(thiophen-2-yl)prop-2-en-1-one		CH ₃	23.55

Graphical abstract



Highlights

- *In our previous study, a compound containing a Michael acceptor was selectively cytotoxic to cancer cells without affecting normal cells.*
- *We designed and synthesized 26 compounds containing a Michael acceptor.*
- *To derive the structural conditions required to obtain stronger cytotoxicity against cancer cells, the relationships between the half-maximal cell growth inhibitory concentration values of the synthesized compounds and their physicochemical properties were evaluated.*
- *The compound with the best half-maximal cell growth inhibitory concentration triggered apoptosis through ROS generation, which then led to stimulation of the caspase pathway.*